Petrological Constraints on Crystallization Conditions of Mesoarchean Sanukitoid Rocks, Southeastern Amazonian Craton, Brazil

Marcelo Augusto de Oliveira, Roberto Dall'Agnol, Bruno Scaillet

JOURNAL OF PETROLOGY | VOLUME 51 | NUMBER 10 | PAGES 2121–2148 | 2010 | doi:10.1093/petrology/egq051

Petrological Constraints on Crystallization Conditions of Mesoarchean Sanukitoid Rocks, Southeastern Amazonian Craton, Brazil

MARCELO AUGUSTO DE OLIVEIRA[1,2]*, ROBERTO DALL'AGNOL[1,2] AND BRUNO SCAILLET[3]

[1]GROUP OF RESEARCH ON GRANITE PETROLOGY, INSTITUTO DE GEOCIÊNCIAS (IG), UNIVERSIDADE FEDERAL DO PARÁ (UFPA), CAIXA POSTAL 8608, 66075-900, BELÉM, PARÁ, BRAZIL

[2]PROGRAMA DE PÓS-GRADUAÇÃO EM GEOLOGIA E GEOQUÍMICA (PPGG), IG, UFPA, 66075-900, BELÉM, PARÁ, BRAZIL

[3]CNRS/INSU, UNIVERSITÉ D'ORLÉANS, UNIVERSITÉ FRANÇOIS RABELAIS TOURS, INSTITUT DES SCIENCES DE LA TERRE D'ORLÉANS, 1A RUE DE LA FÉROLLERIE, 45071 ORLÉANS CEDEX 2, FRANCE

RECEIVED JULY 2, 2009; ACCEPTED AUGUST 6, 2010

We report petrological and geochemical data for the 2·87 Ga Rio Maria sanukitoid granodiorite and associated rocks from Mesoarchean granite–greenstone terranes of the eastern Amazonian craton, Brazil. The dominant rocks have granodiorite to subordinate monzogranitic compositions, with minor proportions of intermediate quartz diorites or quartz monzodiorites, in addition to mafic end-members occurring as layered rocks or as enclaves. The mineral assemblage is dominated by amphibole–plagioclase–biotite and epidote minerals, all of inferred magmatic origin, pyroxenes being notably absent. Textural and compositional criteria indicate that amphibole is a principal mineral on the liquidus of all the Rio Maria rocks. Crystallization conditions have been derived from a comparison between natural phase assemblages, proportions and compositions and experimental studies carried out on similar magma compositions. The comparison shows that the parental magmas were water-rich, with more than 7 wt % dissolved H_2O, with crystallization temperatures in the range 950–680°C. The $Mg/(Mg+Fe)$ ratios of both amphibole and biotite indicate fO_2 conditions in the range NNO + 0·5 to NNO + 2·5 (where NNO is nickel–nickel oxide buffer), therefore pointing to both water-rich and oxidizing conditions for sanukitoid magmas. Amphibole compositions indicate emplacement at around 200 MPa, and record a high-pressure stage of magma crystallization around 600–900 MPa. Sanukitoid magmas share two of the principal characteristics of modern arc magmas, elevated redox state and volatile contents, which suggest that they may have formed in a geodynamic environment broadly similar to present-day subduction zones.

KEY WORDS: *Amazonian craton; crystallization conditions; high-Mg granitoids; mineral chemistry; sanukitoid*

INTRODUCTION

Sanukitoid suites have been reported from several cratons (Stern & Hanson, 1991; Smithies & Champion, 2000; Bagai *et al.*, 2002; Moyen *et al.*, 2003; Halla, 2005; Kovalenko *et al.*, 2005) and are now recognized as an important component of Archean terranes (Condie, 2005; Martin *et al.*, 2005). Sanukitoids were formed during the late Archean (2·95–2·54 Ga) and are high-Mg rocks that display geochemical characteristics similar to both mantle- and crust-derived magmatic rocks. Extensive occurrences of sanukitoid rocks were recently identified in the Mesoarchean Rio Maria granite–greenstone terrane of the eastern Amazonian craton (Althoff *et al.*, 2000; Leite, 2001; Souza *et al.*, 2001; Oliveira *et al.*, 2009). This terrane consists predominantly of greenstone belts, tonalite–trondhjemite–granodiorite (TTG) suites and sanukitoid rocks, with subordinate calc-alkaline leucogranites

*Corresponding author. Telephone: +55 91 3201 7477. Fax: +55 91 3201 7474. E-mail: mao@ufpa.br

(Dall'Agnol *et al.*, 2006; Oliveira *et al.*, 2009). The sanukitoid rocks belong to the ~2·87 Ga Rio Maria suite, which is intrusive into the greenstone belts and older TTG series. Granodiorite is the dominant rock type in the Rio Maria suite. It carries amphibole-rich clots and abundant mafic enclaves and, in the Bannach area, which is the focus of this study, has associated intermediate and layered mafic rocks.

The petrogenesis of sanukitoids is currently the subject of intense debate (Smithies & Champion, 2000; Kovalenko *et al.*, 2005; Lobach-Zhuchenko *et al.*, 2008). Their high Mg-number, associated with elevated Cr and Ni contents, indicates a mantle influence and suggests a peridotitic rather than a basaltic source. On the other hand, the relative light rare earth element (LREE) enrichment and high Ba and Sr contents of sanukitoid magmas compared with typical calc-alkaline series could be interpreted as evidence of their crustal origin or, alternatively, of crustal contamination during their evolution. However, the low contents of these elements in the Archean crust do not favor such hypotheses (Taylor & McLennan, 1985; Stern *et al.*, 1989). The isotopic composition of the sanukitoid rocks is also paradoxical, with Nd and Sr isotopes pointing to a mantle origin (Stern & Hanson, 1991; Kovalenko *et al.*, 2005), whereas Pb isotope compositions of K-feldspars argue for a crustal source (Stevenson *et al.*, 1999; Halla, 2005). At present, most researchers agree that both mantle and subduction-related components must play an important role in the petrogenesis of the sanukitoid series and two main hypotheses have been proposed: (1) a two-stage process: during the first stage, the mantle is metasomatized either by melts (Smithies & Champion, 2000) or by aqueous fluids (Kamber *et al.*, 2002), both slab-derived; in the second stage, melting of the enriched mantle produces sanukitoid magmas (Stern & Hanson, 1991); (2) a one-stage process, involving continuous assimilation of mantle peridotite by slab melts ascending through the mantle wedge (Rapp *et al.*, 1999).

In addition to uncertainties about the origin of sanukitoid rocks, their crystallization conditions, including oxidation state, H_2O content and pressure of crystallization, also remain poorly constrained. Over the last 30 years, a number of experimental studies have been performed to provide quantitative constraints on the magmatic evolution of granitoids (Naney & Swanson, 1980; Naney, 1983; Wyllie, 1984; Clemens *et al.*, 1986; Dall'Agnol *et al.*, 1999; Scaillet & Evans, 1999; Klimm *et al.*, 2003; Pichavant *et al.*, 2007). In particular, Scaillet & Evans (1999), Prouteau & Scaillet (2003) and Bogaerts *et al.* (2006) have performed experimental studies on rocks having compositions similar to the dominant rocks of the Rio Maria suite, which are the focus of the present study. Such studies have proven to be of great help not only in the elucidation of the storage conditions of volcanic rocks (e.g. Martel *et al.*, 1999; Scaillet & Evans, 1999), but also for unravelling the evolution of granitoid plutons (e.g. Clemens & Wall, 1981; Clemens *et al.*, 1986; Scaillet *et al.*, 1995; Dall'Agnol *et al.*, 1999; Klimm *et al.*, 2003; Bogaerts *et al.*, 2006).

The aim of this study is to present a geochemical, mineralogical, and petrological description of the Rio Maria suite from the Bannach area to constrain the crystallization conditions, mainly H_2O content, pressure, temperature and fO_2, using available experimental data on similar rock types. This is the first attempt to evaluate the crystallization conditions of sanukitoid magmas.

ANALYTICAL METHODS

Chemical analyses of samples from the Bannach area were performed at ACME-Lab laboratories. Major, minor and trace elements were analyzed by inductively coupled plasma atomic-emission spectroscopy, and REE by inductively coupled plasma mass spectrometry. Major elements have a detection limit of 0·01%, whereas minor and trace elements have a detection limit between 0·01 and 1 ppm. Major and trace element abundances were determined on 0·1 g samples following a lithium metaborate–tetraborate fusion and dilute nitric acid digestion. Loss on ignition (LOI) is by weight difference after ignition at 1000°C.

The compositions of amphibole, biotite and epidote were determined by electron microprobe at the laboratory of the University of São Paulo, using a JEOL superprobe JXA-8600 electron microprobe using the following analytical conditions: 15 kV acceleration voltage, 20 nA sample current, 10 s total counting time.

Bulk magnetic susceptibility values were measured on representative samples of granodiorite and intermediate rocks from the Rio Maria suite in the Bannach area, using SI-1 flat and cylindrical coils in the magnetic petrology laboratory of UFPA.

GEOLOGICAL SETTING AND FIELD RELATIONSHIPS

The aim of this section is to provide a concise overview of the geology of the study area. The Archean Rio Maria suite crops out in several areas of the Rio Maria granite–greenstone terrane, which corresponds to the southern part of the Archean Carajás province in the eastern domain of the Amazonian Craton (Dall'Agnol *et al.*, 2006; Oliveira *et al.*, 2009). The Carajás province is part of the Central Amazonian province (Tassinari & Macambira, 2004) and is divided into two Archean tectonic domains (Fig. 1a), the 2·98–2·86 Ga Rio Maria granite–greenstone terrane (Macambira & Lafon, 1995; Dall'Agnol *et al.*, 2006) and the extension-related Carajás Basin, mainly composed of 2·76–2·55 Ga metavolcanic rocks, banded iron formations and granitoids (Machado *et al.*, 1991;

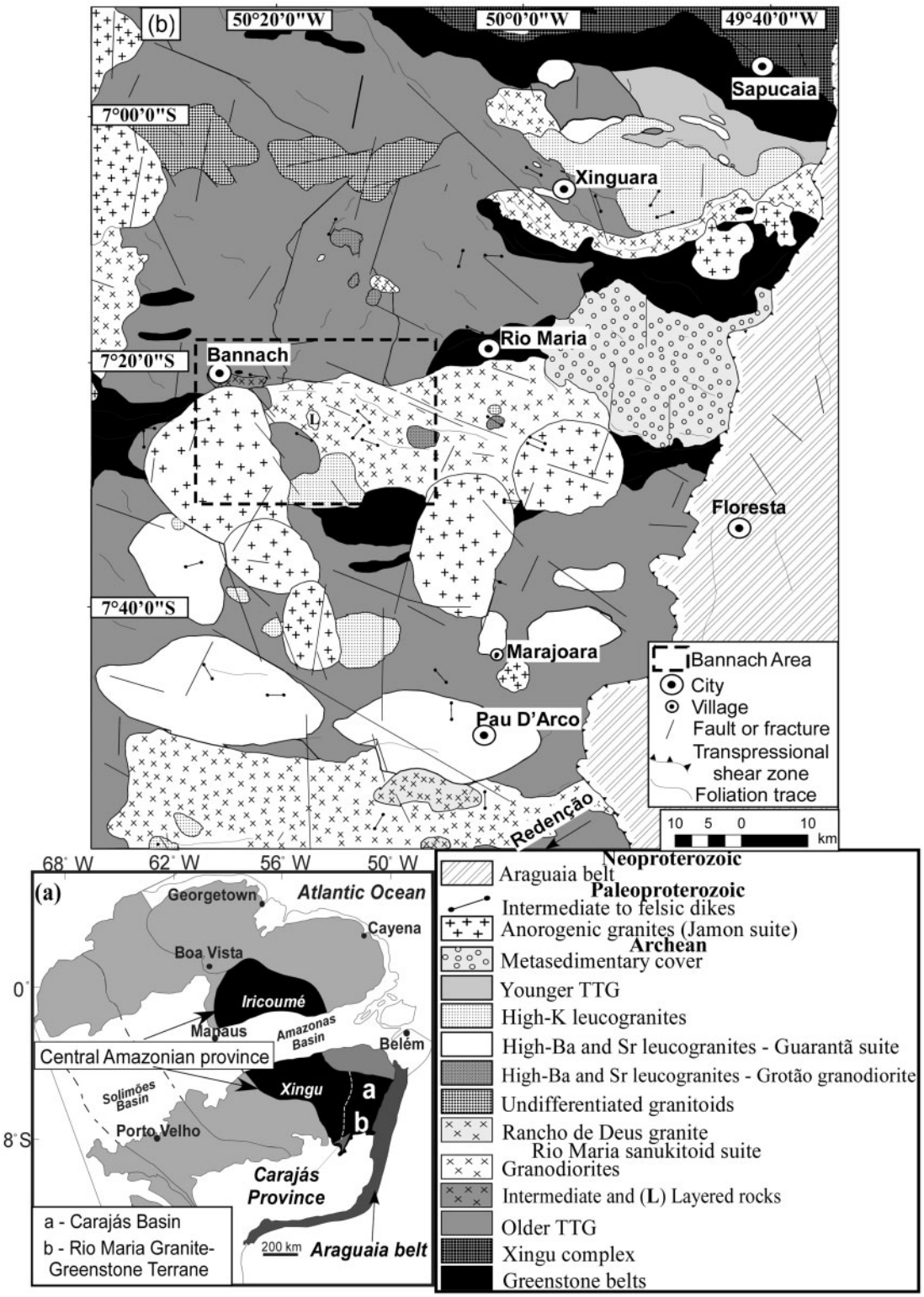

Fig. 1. (a) Location of the studied area in the Amazonian craton; (b) geological map of the Rio Maria granite–greenstone terrane (from Almeida, 2010). Rectangle indicates the location of Fig. 2.

Macambira & Lafon, 1995; Barros *et al.*, 2001). The two domains were cratonized at the end of the Archean and intruded by Paleoproterozoic A-type granites of the Serra dos Carajás and Jamon suite (Dall'Agnol *et al.*, 2005).

The Archean Rio Maria granite–greenstone terrane (Fig. 1) consists of greenstone belts (Andorinhas supergroup, Huhn *et al.*, 1988; Souza *et al.*, 2001) and a number of granitoids (Dall'Agnol *et al.*, 2006). The greenstone belts have ages of 2·97–2·90 Ga and are composed dominantly of metamorphosed tholeiitic basalts and komatiites (Huhn *et al.*, 1988; Souza *et al.*, 2001). The granitoids have yielded ages between 2·98 and 2·86 Ga and are broadly similar to those found in other Archean terranes. Four groups of granitoids can be distinguished: (1) an older TTG series represented by the Arco Verde, Caracol, Mariazinha tonalites, and Mogno trondjemite (~2·98–2·92 Ga; Macambira & Lancelot, 1996; Althoff *et al.*, 2000; Leite *et al.*, 2004; Almeida, 2010); (2) the 2·87 Ga Rio Maria sanukitoid suite formed of various occurrences of granodiorite and associated rock types (Medeiros, 1987; Macambira & Lancelot, 1996; Althoff *et al.*, 2000; Leite *et al.*, 2004; Oliveira *et al.*, 2009); (3) a younger TTG series represented by the Água Fria trondhjemites (2·87 Ga; Leite *et al.*, 2004); (4) ~2·86 Ga Archean granites, including (a) potassic leucogranites of calc-alkaline affinity such as the Xinguara and Mata Surrão plutons (Lafon *et al.*, 1994; Leite *et al.*, 1999, 2004), (b) a leucogranodiorite–granite group represented by the Guarantã suite, Grotão granodiorite and similar granites (Almeida, 2010), and (c) granites associated with sanukitoid suites (Rancho de Deus granite: Almeida, 2010). The principal shearing deformational event identified in this area occurred at around 2·87 Ga (Althoff *et al.*, 2000; Souza *et al.*, 2001; Leite, 2001). The Archean granitoids and greenstone belts are intruded by ~1·88 Ga A-type granite plutons of the Jamon suite and associated dikes (Dall'Agnol *et al.*, 2005; Dall'Agnol & Oliveira, 2007).

Rio Maria granodiorite

The Rio Maria granodiorite is the dominant rock type within the sanukitoid suite, covering large areas (>2000 km^2) of the Rio Maria granite–greenstone terrane (Fig. 1). It is exposed south of Rio Maria (type-area; Medeiros, 1987), to the south and NE of Xinguara (Leite, 2001), to the north of Redenção (Althoff *et al.*, 2000) and to the east of Bannach (Oliveira *et al.*, 2009). Mafic and intermediate sanukitoid rocks are scarce, forming only local occurrences (Xinguara area, Souza, 1994; Leite, 2001) (Fig. 2, Bannach area, Oliveira *et al.*, 2006). Field relationships show that the Rio Maria suite is intrusive into both the greenstone sequences (Souza *et al.*, 2001) and the Arco Verde and Caracol tonalites (Althoff *et al.*, 2000; Leite *et al.*, 2004) and is itself intruded by the Água Fria trondhjemite (Leite *et al.*, 2004), potassic leucogranites (Mata Surrão granite, Duarte, 1992; Xinguara granite, Leite *et al.*, 2004) and by the Paleoproterozoic granites of the Jamon suite (Dall'Agnol *et al.*, 2005).

The Rio Maria granodiorite contains centimeter- to decimeter-scale mafic enclaves and generally has a greenish-gray color owing to the strongly saussuritized plagioclase. It shows a weak subvertical foliation striking WNW–ESE to east–west acquired during late magmatic to high-temperature subsolidus conditions. This foliation is outlined by the preferred orientation of mafic minerals and, locally, enclaves (Althoff *et al.*, 2000; Leite, 2001; Souza *et al.*, 2001). The mafic enclaves have flattened or rounded shapes, being deformed only when located near or along shear zones (Souza, 1994; Althoff *et al.*, 2000; Leite, 2001). The enclaves display evidence of interaction with the host granodiorite, both rocks sharing the same finite strain fabric. These features point to a low viscosity contrast between the enclaves and the Rio Maria granodiorite at the time of enclave incorporation, which suggests coexistence of the two magmas while both were still partly molten (Souza & Dall'Agnol, 1995; Althoff *et al.*, 2000; Leite, 2001).

The Bannach area was selected for this study because of the abundance of mafic and intermediate rocks associated with the Rio Maria granodiorite (Oliveira *et al.*, 2009). The mafic to intermediate rocks occur in two domains (Fig. 2). In the main domain, located near Bannach, they are exposed as part of a stock composed mostly of quartz diorite and quartz monzodiorite; in the second domain, situated along the road between Rio Maria and Bannach, various outcrops of layered rocks can be seen. The dominant intermediate variety consists of mesocratic, dark green rocks, with a medium- to coarse-grained texture. The layered rocks, of inferred cumulate origin (Oliveira, 2005; Oliveira *et al.*, 2009), are characterized by a remarkable concentration of generally quadratic or short prismatic coarse amphibole crystals, set in a matrix of leucocratic intercumulus material. The igneous layering is highlighted by the alternation of darker layers of coarse rocks enriched in centimeter-sized amphibole crystals (Fig. 3c and d), with gray-colored and medium-grained layers. The layering is sub-horizontal, gently dipping northeastward with no evidence of significant superimposed solid-state deformation.

PETROGRAPHY

In the Rio Maria suite the dominant rocks have granodioritic to subordinate monzogranitic (Table 1) composition and display equigranular, medium or coarse even-grained textures (Oliveira, 2005; Oliveira *et al.*, 2009). The associated intermediate rocks are quartz diorites and quartz monzodiorites. All facies of the Rio Maria suite have strongly saussuritized plagioclase and contain amphibole ± biotite ± magmatic epidote as their principal mafic minerals. M (modal % in volume of mafic minerals)

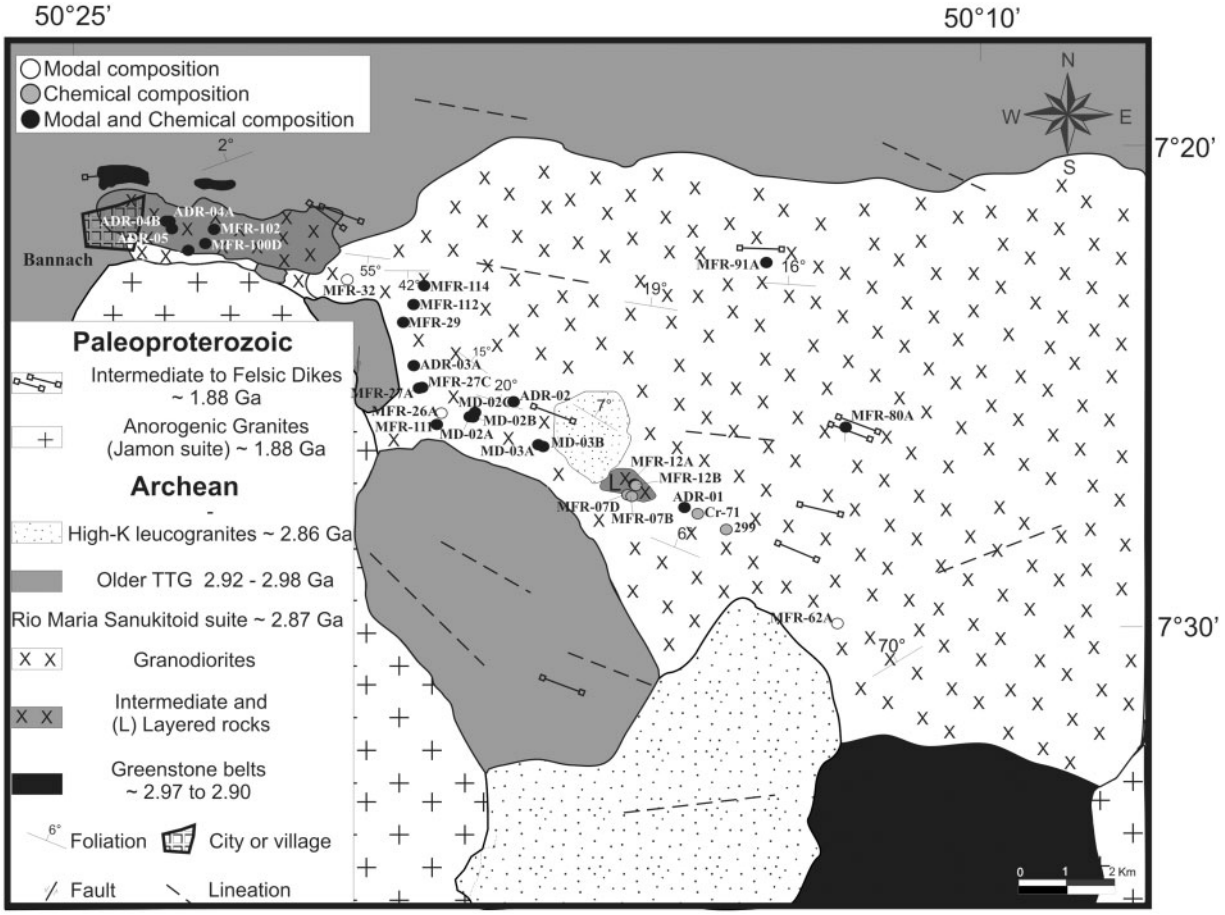

Fig. 2. Geological map of the Bannach area.

values normally vary between 10 and 25% in the granodiorites, attaining higher values (generally 20 to ~40%) in the intermediate rocks (Oliveira *et al.*, 2009). The assemblage of primary accessory minerals includes zircon, apatite, magnetite, titanite, and allanite. In the granodiorites, Fe–Ti oxide minerals are rare to absent, excepting a few samples in which 0·1–0·2% magnetite + ilmenite + hematite modal contents were observed. In the intermediate rocks, opaque mineral modal contents vary from 0·1 to 1·0%, and magnetite and hematite are common accessory phases, which is consistent with their higher magnetic susceptibility (MS) values (mostly $>1 \times 10^{-3}$ SI units) compared with the granodiorites ($<1 \times 10^{-3}$ in SI units; Dias *et al.*, 2006; Nascimento, 2006). In the layered rocks, opaque mineral modal contents are variable but goethite is relatively abundant and magnetite is scarce, explaining the low MS values of these rocks. The layered rocks display MS values that, in most cases, overlap those of the intermediate rocks with the lowest MS values. The intermediate rocks can be classified as magnetite-series granitoids, according to the terminology of Ishihara (1977, 1981). However, assuming that the present-day iron–titanium oxide assemblage is representative of the magmatic stage of evolution, the granodiorite would be more akin to the ilmenite-series of Ishihara (but see below). The magnetic behavior of the layered rocks is also ambiguous, but they are more similar to the intermediate rocks than the granodiorite.

In the dominant epidote–biotite–hornblende granodiorite, microscope-scale textural criteria indicate that apatite, zircon, magnetite and allanite are early crystallized phases followed by magnesian hornblende and plagioclase (Oliveira, 2005; Oliveira *et al.*, 2009). Amphibole forms euhedral, twinned crystals, which are well preserved or only partially replaced by late magmatic biotite and subordinate titanite and epidote. Plagioclase is euhedral to subeuhedral and originally zoned but the intense saussuritization prevents the determination of its original composition. Biotite crystallizes after both amphibole and plagioclase and displays regular contacts with euhedral epidote suggesting equilibrium between these two minerals. Such epidotes exhibit, however, highly embayed,

Fig. 3. (a, b) Field aspects of the Rio Maria granodiorite, showing elongated (a) and rounded (b) mafic enclaves; (c, d) outcrop of the layered rocks of Bannach area; (e, f) hand samples of a layered rock displaying dark color and well-preserved centimeter-sized euhedral amphibole crystals.

irregular contacts with quartz and plagioclase. In addition to secondary epidote derived from plagioclase, two textural types of epidote interpreted as of magmatic origin can be distinguished: (1) epidote with an allanite core and (2) zoned epidote associated with, and partially enclosed by, biotite. In all rocks of the Rio Maria suite, modal abundances of magmatic epidote are as high as 5 vol. %. Quartz forms subhedral to anhedral medium-grained crystals that are sometimes recrystallized, forming subgrains with undulatory extinction. K-feldspars crystallized late,

Table 1: Modal composition (determined by point counting) of the rocks of Rio Maria suite (Bannach area)

	Layered	Mafic enclaves[1]								Intermediate rocks[2]		Granodiorites[2]			
Facies:	Dark layer	EBAD	EBAMzD		EBAQMzD		EBAQMz			EBAQD	EBAQMzD	EBAGD			
Sample:	MFR-12B	MFR-27C	ADR-2	MD-2D	MD-2C	MD-3A	MD-2F	MD-2A	MD-2B	ADR-4B	ADR-5	MFR-32	MFR-80A	MFR-114	ADR-3A
Plagioclase	24·1	48·4	44·9	39·1	31·5	34·0	24·9	23·8	23·4	47·1	51·7	49·7	48·2	46·6	36·8
Alkali-feldspar	n.d.	0·6	14·6	13·0	12·3	9·6	14·9	18·7	22·1	4·3	6·7	15·9	9·1	9·3	15·2
Quartz	6·9	2·5	0·7	1·8	2·8	7·5	2·9	5·2	5·3	13·0	13·7	16·1	20·5	19·2	23·2
Amphibole	52·6	37·6	33·4	34·2	41·3	37·4	47·0	46·7	40·1	28·7	20·3	9·8	8·2	12·7	11·1
Biotite	7·7	7·9	3·3	7·1	5·5	7·0	5·3	3·1	4·5	0·7	4·5	4·4	7·2	8·2	7·5
Epidote[m]	1·8	1·5	0·6	2·4	1·6	0·6	1·3	1·5	1·5	1·5	0·6	1·2	1·9	1·1	1·8
Epidote[s]	0·3	0·9	0·5	0·3	0·2	0·2	0·3	0·1	0·2	0·3	0·5	1·1	2·6	0·8	2·0
Opaque minerals	0·6	–	0·3	1·6	4·0	3·5	3·3	0·6	2·3	1·1	0·8	–	n.d.	0·1	n.d.
Titanite	0·6	0·2	0·3	0·2	0·4	0·2	0·1	0·1	0·6	1·5	0·5	0·6	0·7	0·7	0·9
Apatite	0·6	0·3	0·1	–	–	–	–	–	–	0·7	0·2	0·2	0·8	0·2	0·2
Allanite	1·2	0·2	–	–	–	–	–	–	–	1·0	0·4	0·3	n.d.	n.d.	0·1
Carbonate	0·7	–	–	–	–	–	–	–	–	n.d.	n.d.	–	–	–	–
Felsic	31	51·5	60·2	53·9	46·6	51·1	42·7	47·7	50·8	64·4	72·1	81·7	77·8	75·1	75·2
Mafic	69	48·6	38·5	45·8	53·0	48·9	57·3	52·1	49·2	35·5	27·8	17·6	21·4	23·8	23·6

Data sources: [1]this paper; [2]Oliveira (2005). E, epidote; B, biotite; A, amphibole; Q, quartz; D, diorite; MzD, monzodiorite; Mz, monzonite; GD, granodiorite; [m]magmatic; [s]secondary. n.d., not determined.

forming anhedral, sometimes poikilitic crystals, with inclusions of quartz, plagioclase and euhedral amphibole. At the subsolidus stage, chlorite, secondary epidote, sericite and carbonates were produced.

In the quartz diorites and quartz monzodiorites, the mineral assemblages and textural relationships between the minerals are very similar to those observed in the dominant granodiorite, amphibole and plagioclase being more abundant whereas quartz and K-feldspars modal contents are lower than in the granodiorite.

The mineralogy of the layered rocks is similar to that of the Rio Maria granodiorite and intermediate rocks. The textural variations are directly related to the layers of the rock. The darker layers have an inequigranular texture and the cumulus material is formed of centimeter-sized euhedral pargasite to magnesium-hornblende crystals (Fig. 3e and f) with rims of magnesium-hornblende to actinolitic hornblende, partially replaced by biotite. The intercumulus material is mainly composed of quartz and intensely saussuritized plagioclase, with subordinate amphibole, biotite, and epidote. The accessory minerals are allanite, titanite, magnetite, and apatite. The gray layers also have an inequigranular texture. In these layers, the cumulus material is composed of comparatively smaller amphibole crystals whose replacement by biotite is more intense when compared with the darker layers. The intercumulus phases are similar to those observed in the darker layers.

For a more detailed study of the mafic enclaves, samples were drilled out at four localities with a portable drill core. The central parts of the cores exhibit no apparent interaction with the host granodiorite and are laminated. Such cores have dioritic to quartz monzonitic composition (see Käpyaho, 2006) and follow a monzonitic trend in the QAP plot (Fig. 4) (Lameyre & Bowden, 1982). The textures in the dioritic enclaves are not particularly different from those of the intermediate Rio Maria rocks. In the monzodiorites to quartz monzonites, the presence of abundant poikilitic coarse K-feldspar crystals with inclusions of medium- to fine-grained amphibole is noteworthy. The alkali-feldspar crystals are sub-euhedral and display regular contacts with plagioclase. Textural evidence indicates that they crystallized in equilibrium with the other minerals and do not correspond to entrained crystals from the enclosing granodiorite. These enclaves are rich in mafic minerals with $M \geq 40\%$ (Fig. 4). Amphibole is by far the most abundant mafic mineral, followed by biotite, magmatic epidote, and the same accessory mineral assemblage as the granodiorite. The amphibole crystals are generally euhedral and contain minute inclusions of opaque minerals. Quartz modal contents are low and crystals are anhedral, filling the interstices between other minerals,

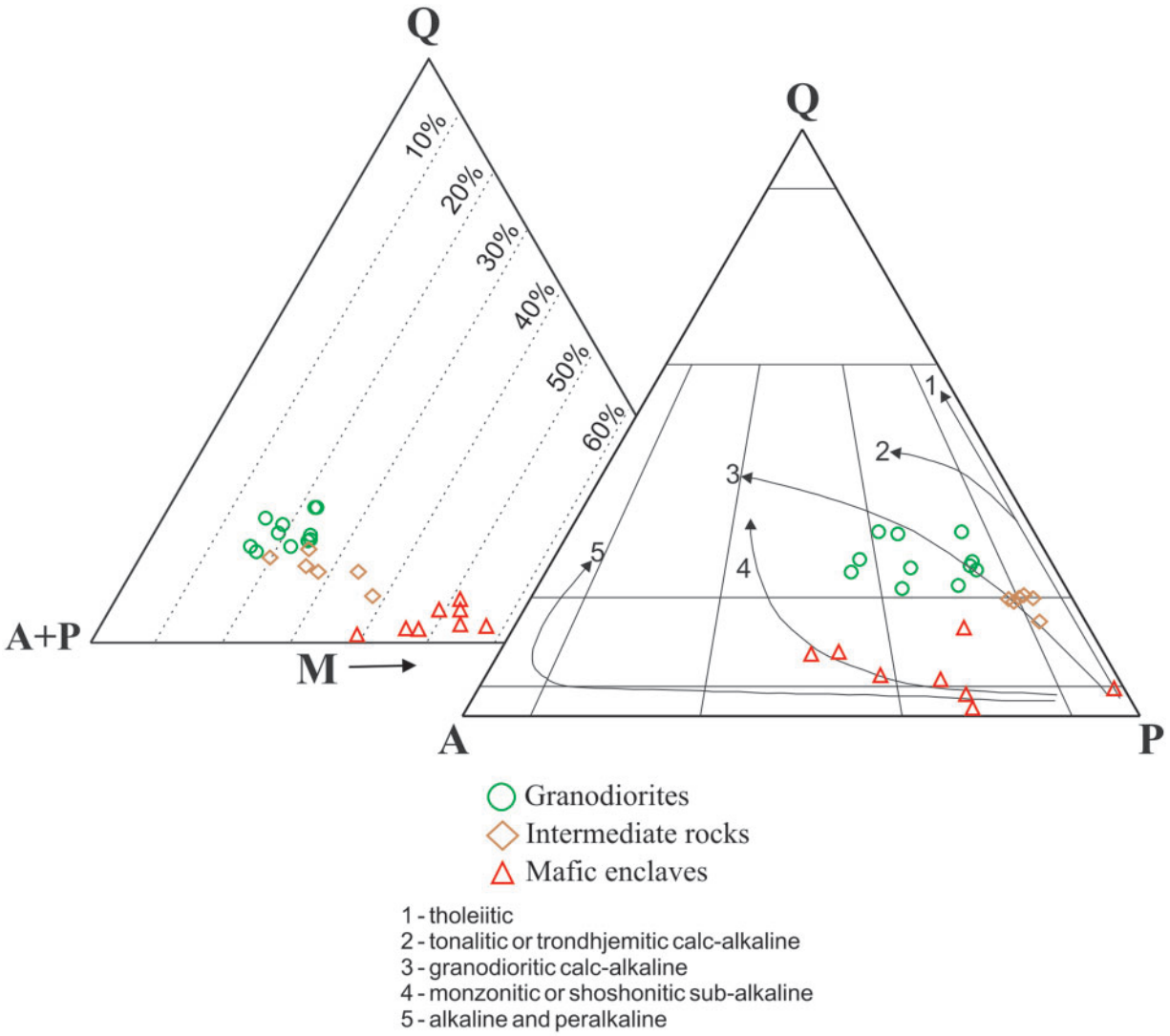

Fig. 4. QAP and Q–(A + P)–M plots for the rocks of the Rio Maria suite (Bannach area). Data sources: granodiorites and intermediate rocks from Oliveira (2005); mafic enclaves, this study.

suggesting late crystallization. The contacts between the enclaves and the host granodiorite are sharp but indented in detail. Amphibole crystals are concentrated along the contact and the ratio of plagioclase/K-feldspar is greater towards the edge of the enclave.

The key feature relevant to the estimation of crystallization conditions is the occurrence of magmatic amphibole and epidote, both minerals being diagnostic of specific P–T–H_2O–fO_2 conditions as indicated below. In particular, the early appearance of amphibole in the crystallization sequence and its elevated modal proportion in the entire suite strongly suggest that conditions conducive to massive precipitation of this mineral were dominant during pluton solidification. In this respect, we note that experiments have shown that very high modal proportions of amphibole, over 60 wt %, can be reached during crystallization of hydrous basaltic magmas in the mid- to lower crust (Pichavant & Macdonald, 2007). In other words, a high modal proportion of a particular mineral in a plutonic rock need not reflect an accumulation processes only: it may also be a primary feature of the solidified magmatic rock.

GEOCHEMISTRY

A detailed discussion of the geochemistry of the studied rocks and of their sanukitoid affinity has been given by Oliveira *et al.* (2009). Below we provide an overview of the major geochemical characteristics of the Rio Maria sanukitoids.

The sanukitoid character of the four groups of rocks (i.e. layered rocks, mafic enclaves, intermediate rocks and granodiorites) is indicated by their metaluminous compositions, high Mg-number values (Fig. 5), high Cr and Ni contents (Fig. 5), in addition to elevated contents of large ion lithophile elements (LILE), especially Ba and Sr (Table 2). The layered rocks and mafic enclaves have similar silica contents, which vary from 50 to 57 wt % (Table 2), compared with the intermediate rocks and granodiorites (respectively, 59–64 wt % and 63–67 wt %). The Al_2O_3 contents are similar in the enclaves, intermediate rocks and granodiorites, reaching the lowest values in the layered rocks, which are impoverished in feldspars relative to the other members of the suite. All analyzed rocks have Al_2O_3 contents (Table 2) that are lower than those of typical calc-alkaline series of similar silica contents (Irvine & Baragar, 1971; Ringwood, 1975; Wilson, 1989).

The REE patterns of the granodiorites and intermediate rocks are similar, with pronounced enrichment in the LREE and strong to moderate fractionation of the heavy rare earth elements (HREE), associated with small or absent Eu anomalies. The REE patterns in the layered rocks and enclaves show a less pronounced enrichment in LREE, and minor fractionation of HREE relative to the granodiorites and intermediate rocks. Despite these geochemical similarities, Oliveira *et al.* (2009) have shown that the granodiorites and intermediate rocks probably derived from two distinct magmas, both with sanukitoid affinity, which possibly originated from different degrees of partial melting of a metasomatized mantle source.

MINERAL COMPOSITIONS

Amphibole

The amphibole was analyzed in one sample from each of granodiorite, intermediate rock, mafic enclave, and on two samples of layered rocks (Table 3). According to the classification of Leake *et al.* (1997), the amphibole within the Rio Maria suite is a Mg-hornblende; subordinate pargasite and Mg-hastingsite occur in the layered rocks and mafic enclaves (Fig. 6). The amphibole rims are enriched in silica and impoverished in alumina relative to the cores, with Mg-hornblende to actinolitic hornblende compositions, the latter being found only in the intermediate rocks and in the cumulate crystals of the layered rocks (Fig. 6). Amphibole Fe/(Fe + Mg) ratios (Fe-number) range from 0·25 to 0·43 in the rocks of the Rio Maria suite (Table 3; Fig. 7); the lowest values are found in the cores of the amphibole cumulus crystals in the layered rocks (0·25–0·33; Fig. 7a and b). The Fe-number of the amphibole cores increases gradually from the intermediate rocks to the intercumulate layered rocks (respectively, 0·29–0·35 and 0·28–0·40). The highest Fe-number values are found in the amphibole core of enclaves (0·37–0·43)

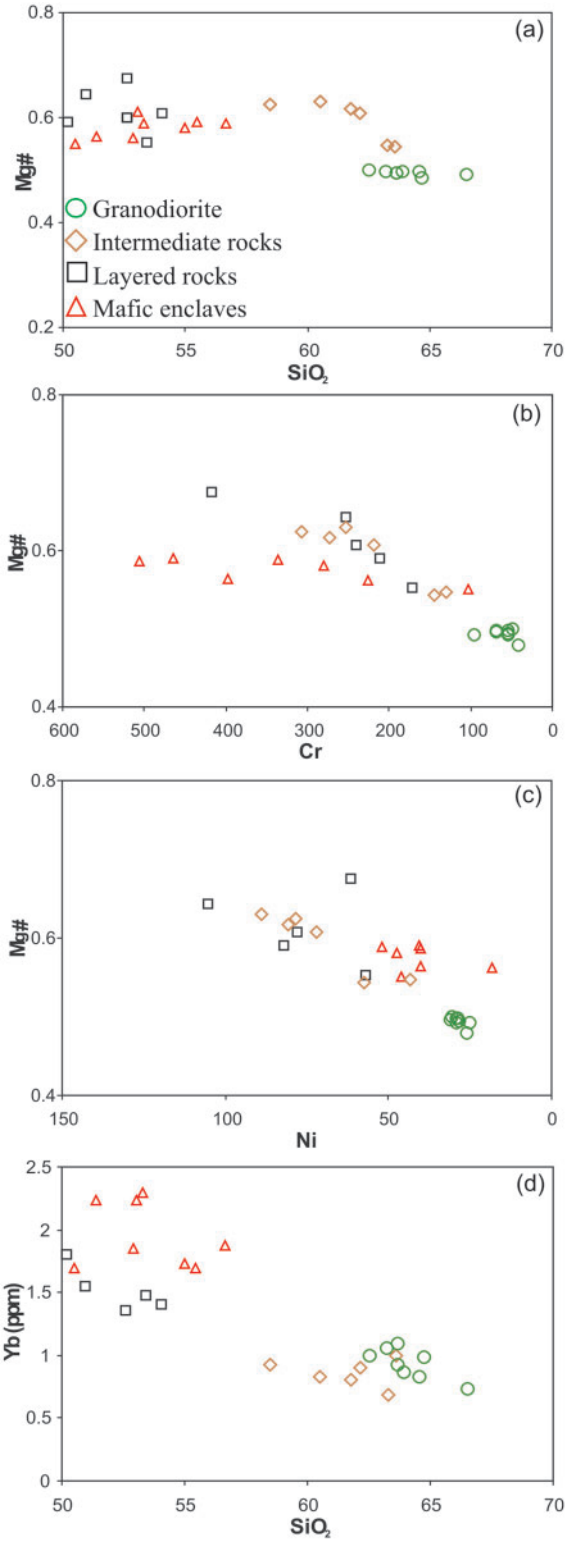

Fig. 5. (a) Mg-number vs SiO_2; (b) Mg-number vs Cr; (c) Mg-number vs Ni; (d) Yb vs SiO_2 diagrams for the rocks of the Rio Maria suite (Bannach area).

Table 2: Chemical composition of the samples of the Rio Maria suite (Bannach area)

	Layered rocks[1]						Mafic enclaves[2]							
Facies:	Dark layer			Gray layer			EBAD to EBAQMz							
Sample:	MFR-07B	MFR-12B	ADR-1	MFR-07D	Cr-71	MFR-12A	MFR-27C	MD-02C	MD-03A	299	MD-02A	ADR-2	MD-02B	MD-03B
SiO_2 (wt %)	50·92	52·60	54·04	50·14	52·60	53·41	50·51	51·38	52·89	53·03	53·3	54·98	55·46	56·64
TiO_2	0·73	0·56	0·63	0·97	0·70	0·78	0·88	0·72	0·69	0·72	0·69	0·61	0·55	0·85
Al_2O_3	12·11	10·91	13·02	13·08	13·21	14·76	16·19	13·77	15·63	13·56	12·29	14·34	13·09	13·28
Fe_2O_3	4·16	3·28	3·41	3·63	11·89	4·07	5·06	11·15	9·58	10·49	10·2	3·59	8·94	9·05
FeO	5·96	5·96	3·41	7·08	n.d.	4·83	4·46	n.d.	n.d.	n.d.	n.d.	4·14	n.d.	n.d.
MnO	0·15	0·15	0·13	0·15	0·15	0·13	0·13	0·2	0·17	0·18	0·19	0·14	0·17	0·16
MgO	9·94	10·51	7·37	8·48	9·17	5·98	5·65	7·38	6·28	8·39	7·43	5·82	6·61	6·61
CaO	8·21	9·3	8·15	8·81	8·55	7·88	7·61	8·36	7·66	7·79	7·42	6·73	6·24	6·52
Na_2O	2·49	2·06	2·86	2·60	2·36	2·99	4·06	3·53	4·72	2·87	2·31	3·86	2·59	3·83
K_2O	2·04	1·03	1·74	1·72	1·94	2·00	2·33	1·94	1·1	2·32	4·23	3·07	4·96	1·76
P_2O_5	0·22	0·15	0·17	0·17	0·24	0·23	0·45	0·37	0·33	0·25	0·31	0·27	0·29	0·31
LOI	2·10	2·50	2·30	2·00	n.d.	2·10	1·90	0·8	0·6	n.d.	1·2	1·6	0·6	0·6
Total	99·03	99·01	99·10	98·83	100·81	99·16	99·23	99·56	99·65	99·60	99·57	99·15	99·50	99·61
Ba (ppm)	511	442	527	608	n.d.	711	344	468	199	1145	1088	876	1382	417
Rb	118	39	80	77	115	84	140	89	56	98	125	94	101	77
Sr	477	335	507	494	422	604	800	508	544·8	445	357·7	463	338	436
Zr	97	81	92	87	116	99	165	140	151	129	118	105	103	153
Nb	5	4	5	5	5	5	7	8	7	11	11	11	7	7
Y	17	17	17	23	15	19	23	23	22	24	25	23	19	23
Ga	17	14	17	18	n.d.	20	25	19	20	n.d.	16	20	15	17
Th	8	6	6	6	n.d.	6	1	2	2	n.d.	2	5	2	3
Ni	105	61	80	82	n.d.	57	46	40	18	n.d.	40	47	40	52
Cr	253	417	239	212	n.d.	171	103	397	226	n.d.	506	281	465	335
La	33	24·3	25·4	31·8	n.d.	27·6	28·5	25·0	25·4	n.d.	22·4	29	18·4	30·8
Ce	62·8	43·7	55·2	67·2	n.d.	53·9	77·1	67·2	60·4	n.d.	64·8	72·1	50·2	71·0
Pr	6·47	5·28	5·69	6·97	n.d.	6·54	10·11	10·41	9·85	n.d.	10·43	9·42	7·99	10·41
Nd	25·1	20·9	24·5	28·9	n.d.	27·1	44	41·6	43·5	n.d.	43·00	40·4	32·8	41·8
Sm	4·80	4·10	4·5	6·1	n.d.	5·3	8·6	8·4	8·35	n.d.	8·61	7·5	6·62	7·91
Eu	1·29	1·14	1·33	1·69	n.d.	1·59	1·73	1·58	1·62	n.d.	1·75	1·52	1·27	1·59
Gd	4·04	3·59	3·64	5·06	n.d.	4·74	5·71	6·65	6·64	n.d.	6·92	5·8	5·4	6·7
Tb	0·6	0·51	0·58	0·82	n.d.	0·72	0·86	0·97	0·88	n.d.	0·96	0·98	0·74	0·88
Dy	2·82	2·79	2·89	3·9	n.d.	3·37	4·35	4·94	4·36	n.d.	4·66	4	3·83	4·5
Ho	0·54	0·53	0·6	0·77	n.d.	0·69	0·78	0·87	0·81	n.d.	0·87	0·74	0·71	0·8
Er	1·51	1·52	1·68	2·14	n.d.	1·82	2·05	2·41	2·14	n.d.	2·33	2·04	1·88	2·16
Tm	0·23	0·24	0·19	0·33	n.d.	0·26	0·29	0·37	0·32	n.d.	0·38	0·27	0·28	0·35
Yb	1·55	1·36	1·41	1·8	n.d.	1·48	1·7	2·24	1·85	n.d.	2·3	1·73	1·69	1·88
Lu	0·22	0·2	0·23	0·3	n.d.	0·25	0·25	0·32	0·28	n.d.	0·34	0·29	0·26	0·28
$\sum$REE	144·97	110·16	127·84	157·78	n.d.	135·36	186·03	172·96	166·4	n.d.	169·75	175·79	132·07	181·06
$(La/Yb)_n$	14·37	12·06	12·16	11·92	n.d.	12·59	11·32	7·53	9·27	n.d.	6·57	11·31	7·35	11·06
$(La/Sm)_n$	4·33	3·73	3·55	3·28	n.d.	3·28	2·09	1·87	1·92	n.d.	1·64	2·43	1·75	2·45
$(Dy/Yb)_n$	1·18	1·33	1·33	1·41	n.d.	1·48	1·66	1·43	1·53	n.d.	1·32	1·5	1·47	1·56
Eu/Eu*	0·9	0·91	1·0	0·93	n.d.	0·97	0·75	0·65	0·67	n.d.	0·69	0·7	0·65	0·67
Rb/Sr	0·25	0·12	0·16	0·16	0·27	0·14	0·17	0·18	0·10	0·22	0·35	0·20	0·30	0·18
Sr/Ba	0·93	0·76	0·96	0·81	n.d.	0·85	2·32	1·09	2·74	0·39	0·33	0·53	0·24	1·04
K/Na	0·54	0·33	0·40	0·44	0·54	0·44	0·38	0·36	0·15	0·53	1·20	0·52	1·26	0·30
$FeO_t/(FeO_t + MgO)$	0·49	0·46	0·47	0·55	0·54	0·59	0·61	0·58	0·58	0·53	0·55	0·56	0·55	0·55
Mg-no.	0·64	0·67	0·61	0·59	0·60	0·55	0·55	0·56	0·56	0·61	0·59	0·58	0·59	0·59

(continued)

Table 2: Continued

Facies:	Intermediate rocks[3] EBAQzD to EBAQzMD						Granodiorites[3] EBAGD to EBAMzG							
Sample:	ADR-4A	ADR-4B	ADR-5	MFR-102	MFR-100D	ADR-7	MFR-114	MFR-27	MFR-111	MFR-29	ADR-3A	MFR-112	MFR-91A	MFR-80A
SiO_2 (wt %)	58·47	60·51	61·75	62·15	63·29	63·61	62·52	63·23	63·66	63·66	63·9	64·58	64·72	66·49
TiO_2	0·47	0·44	0·43	0·39	0·38	0·37	0·46	0·49	0·42	0·45	0·43	0·42	0·39	0·33
Al_2O_3	14·02	14·03	13·96	14·5	14·97	14·94	15·23	14·82	14·87	14·84	14·82	14·65	14·98	14·55
Fe_2O_3	2·46	2·37	2·89	2·34	2·51	3·12	2·91	2·8	2·81	3·00	2·91	2·86	2·71	2·27
FeO	3·94	3·43	2·44	2·56	1·96	1·41	1·97	1·89	1·64	1·48	1·65	1·47	1·49	1·32
MnO	0·09	0·09	0·07	0·07	0·06	0·06	0·07	0·06	0·06	0·06	0·06	0·06	0·06	0·05
MgO	5·81	5·37	4·62	4·11	2·89	2·86	2·61	2·49	2·31	2·31	2·39	2·28	2·06	1·85
CaO	5·88	4·73	4·84	4·65	4·18	4·03	4·4	4·36	3·99	4·17	4·02	3·77	4·08	3·02
Na_2O	3·77	4·04	3·98	4·21	4·36	4·4	4·3	4·21	4·19	4·09	4·05	4·04	4·29	4·13
K_2O	2·21	2·16	2·31	2·24	2·57	2·66	2·93	3·01	3·32	3·22	3·21	3·44	2·98	3·75
P_2O_5	0·17	0·18	0·16	0·14	0·15	0·13	0·17	0·15	0·15	0·14	0·14	0·15	0·12	0·14
LOI	1·9	1·9	1·9	2·00	2·00	1·8	1·6	1·8	1·9	1·9	1·8	1·5	1·5	1·4
Total	99·19	99·25	99·35	99·36	99·32	99·39	99·17	99·31	99·32	99·32	99·38	99·22	99·38	99·3
Ba (ppm)	812	701	847	830	1008	1090	1139	1175	1052	1022	1098	1064	1044	1089
Rb	73	72	72	74	87	82	98	103	113	112	109	122	101	116
Sr	745	618	724	828	872	905	692	661	615	611	576	567	632	512
Zr	94	94	101	94	95	103	113	126	103	131	109	110	113	122
Nb	6	5	6	5	6	7	8	9	8	8	7	11	9	10
Y	11	10	11	10	10	12	16	13	11	15	11	12	17	12
Ga	18	18	19	20	20	20	20	20	19	20	20	19	20	19
Th	3	2	5	5	6	5	7	7	7	8	5	11	8	12
Ni	79	89	81	72	43	57	31	29	28	29	31	29	26	25
Cr	308	253	274	219	130	144	48	68	55	96	68	55	41	55
La	23·7	23·3	25·1	25·2	42·2	33·8	37·3	36·9	33·7	34·3	20·0	40·7	53·5	48·0
Ce	51·1	50·3	51·4	47·6	68·3	58·6	72·8	71·9	64·1	64·1	45·7	70·8	72·2	64·2
Pr	5·35	5·35	5·3	5·35	7·37	7·35	7·19	7·57	6·32	6·53	4·94	7·04	8·51	6·81
Nd	21·4	21·4	19·3	20·8	26·1	29·2	27·2	27·8	22·9	24·7	21·7	25·6	31·6	23·9
Sm	3·6	3·4	3·3	3·6	4·1	4·3	4·4	4·9	3·7	4·3	3·7	3·9	4·5	3·4
Eu	1·02	0·95	0·98	0·99	1·05	1·23	1·25	1·35	1·06	1·14	1·05	1·07	1·3	0·95
Gd	2·78	2·49	2·58	2·42	2·82	3·19	3·47	3·56	2·9	3·2	2·63	2·71	3·37	2·43
Tb	0·45	0·37	0·37	0·4	0·35	0·48	0·56	0·53	0·42	0·47	0·41	0·4	0·52	0·36
Dy	2·25	1·84	1·98	1·75	1·67	2·2	2·41	2·19	1·92	2·19	1·86	1·9	2·31	1·56
Ho	0·38	0·34	0·33	0·34	0·31	0·42	0·48	0·42	0·34	0·42	0·41	0·4	0·49	0·32
Er	1·03	0·97	0·88	0·95	0·78	1·13	1·3	1·15	0·92	1·19	1·02	0·92	1·25	0·81
Tm	0·13	0·1	0·1	0·1	0·11	0·13	0·14	0·17	0·11	0·17	0·1	0·23	0·17	0·12
Yb	0·93	0·83	0·81	0·9	0·69	1·00	1·00	1·06	0·92	1·09	0·87	0·83	0·99	0·73
Lu	0·15	0·14	0·12	0·13	0·12	0·15	0·16	0·16	0·11	0·15	0·14	0·15	0·15	0·13
∑REE	114·27	111·78	112·55	110·53	155·97	143·18	159·66	159·66	139·42	143·95	104·53	156·65	180·86	153·72
$(La/Yb)_n$	17·20	18·95	20·92	18·90	41·28	22·81	25·18	23·50	24·72	21·24	15·52	33·10	36·48	44·38
$(La/Sm)_n$	4·14	4·31	4·79	4·41	6·48	4·95	5·34	4·74	5·73	5·02	3·4	6·57	7·49	8·89
$(Dy/Yb)_n$	1·57	1·44	1·59	1·26	1·57	1·43	1·57	1·34	1·36	1·31	1·39	1·49	1·52	1·39
Eu/Eu*	0·99	1·00	1·03	1·03	0·94	1·02	0·98	0·99	0·99	0·94	1·03	1·01	1·02	1·01
Rb/Sr	0·1	0·12	0·1	0·09	0·1	0·09	0·14	0·16	0·18	0·18	0·19	0·22	0·16	0·23
Sr/Ba	0·92	0·88	0·85	1·00	0·86	0·83	0·61	0·56	0·58	0·6	0·53	0·53	0·61	0·47
K/Na	0·39	0·35	0·38	0·35	0·39	0·40	0·45	0·47	0·52	0·52	0·52	0·56	0·46	0·60
$FeO_t/(FeO_t + MgO)$	0·52	0·51	0·52	0·53	0·59	0·60	0·64	0·64	0·64	0·64	0·64	0·64	0·66	0·65
Mg-no.	0·62	0·63	0·62	0·61	0·55	0·54	0·50	0·50	0·50	0·49	0·49	0·50	0·48	0·49

Data sources: [1]Oliveira (2005); [2]this paper; [3]Oliveira *et al.* (2009). Chemical ratios: Mg-number is molecular ratio Mg/(Mg + Fe); K/Na molecular ratio. $Eu/Eu^* = Eu_N/[0{\cdot}5 \times (Sm_N + Gd_N)]$. E, epidote; B, biotite; A, amphibole; Qz, quartz; D, diorite; MzD, monzodiorite; Mz, monzonite; GD, granodiorite; MzG, monzogranite.

Table 3: Representative electron microprobe analyses of amphibole from the Rio Maria suite (Bannach area)

Facies:	Layered rocks								Mafic enclaves				Intermediate rocks				Granodiorites			
	Cumulate crystals				Intercumulate crystals				EBAD				EBAQzD				EBAGD			
Sample:	MFR-12B				MFR-12B				MFR-27C				ADR-4B				ADR-3A			
	core	core	rim	rim	core	core	rim	rim	core	core	rim	rim	core	core	rim	rim	core	core	rim	rim
SiO_2 (wt %)	43·359	43·462	49·884	50·349	48·997	49·440	47·834	49·941	47·012	47·555	47·609	47·767	48·356	49·088	49·839	50·549	47·501	47·923	48·602	49·367
TiO_2	1·592	1·274	0·522	0·395	0·538	0·392	0·533	0·421	1·063	0·986	1·170	1·024	0·469	0·454	0·518	0·162	0·918	0·462	0·554	1·030
Al_2O_3	11·685	11·862	5·736	5·245	5·887	5·858	6·963	5·349	6·980	6·683	7·048	6·501	5·964	5·619	4·942	4·741	7·362	7·227	6·581	5·968
FeO	10·417	10·314	11·219	11·727	13·015	12·919	13·218	12·395	15·372	15·187	15·349	15·768	13·852	13·453	13·537	12·496	14·920	15·012	15·429	13·118
MnO	0·131	0·140	0·186	0·247	0·227	0·234	0·223	0·238	0·348	0·310	0·343	0·332	0·281	0·274	0·329	0·267	0·346	0·348	0·351	0·349
MgO	14·910	14·961	15·592	15·232	14·306	14·651	14·139	15·066	12·993	12·943	13·053	13·353	13·900	14·573	14·780	15·109	12·576	13·006	13·342	14·423
CaO	12·611	12·482	13·046	13·075	12·635	12·847	12·513	12·843	12·229	12·420	12·209	12·355	12·435	12·069	11·811	12·678	12·269	12·383	12·376	12·234
Na_2O	1·771	1·551	0·646	0·582	0·929	0·775	0·873	0·688	1·091	0·833	0·918	0·930	0·879	0·915	0·711	0·636	0·940	0·741	1·002	0·960
K_2O	0·836	0·805	0·404	0·356	0·453	0·383	0·523	0·334	0·741	0·663	0·704	0·678	0·474	0·447	0·406	0·294	0·684	0·581	0·537	0·490
F	0·119	0·005	n.d.	n.d.	n.d.	n.d.	0·113	0·070	0·033	0·004	0·116	0·000	0·115	0·079	0·076	0·148	0·456	0·116	n.d.	n.d.
Cl	0·018	0·018	n.d.	0·026	n.d.	0·023	0·034	0·018	0·049	0·067	0·054	0·034	0·052	0·060	0·112	0·026	0·031	0·044	0·036	0·016
O–F–Cl	0·050	0·010	n.d.	n.d.	n.d.	n.d.	0·060	0·030	0·020	0·020	0·060	0·010	0·060	0·050	0·060	0·070	0·200	0·060	n.d.	n.d.
Total	97·450	96·870	n.d.	n.d.	n.d.	n.d.	96·970	97·360	97·910	97·650	98·570	98·740	96·780	97·030	97·060	97·110	98·010	97·840	n.d.	n.d.
Structural formulae as 13-CNK																				
Si	6·307	6·317	7·220	7·309	7·178	7·183	7·006	7·247	6·902	6·991	6·925	6·933	7·121	7·150	7·225	7·346	6·987	6·998	7·031	7·136
Al^{IV}	1·693	1·683	0·780	0·691	0·822	0·817	0·994	0·753	1·098	1·009	1·075	1·067	0·879	0·850	0·775	0·654	1·013	1·002	0·969	0·864
Fe^{3+}	0·450	0·582	0·166	0·101	0·195	0·257	0·396	0·251	0·459	0·368	0·492	0·569	0·355	0·529	0·651	0·279	0·285	0·466	0·479	0·340
Al^{VI}	0·309	0·348	0·198	0·206	0·194	0·185	0·207	0·161	0·108	0·148	0·132	0·044	0·155	0·114	0·068	0·157	0·262	0·241	0·153	0·152
Ti	0·174	0·139	0·057	0·043	0·059	0·043	0·059	0·046	0·117	0·109	0·128	0·112	0·052	0·050	0·056	0·018	0·102	0·051	0·060	0·112
Mg	3·233	3·242	3·364	3·297	3·124	3·173	3·087	3·259	2·844	2·837	2·830	2·889	3·052	3·164	3·194	3·273	2·758	2·831	2·877	3·108
Fe^{2+}	0·818	0·672	1·192	1·323	1·400	1·313	1·223	1·254	1·429	1·500	1·375	1·345	1·351	1·110	0·990	1·239	1·551	1·368	1·388	1·246
Mn	0·016	0·017	0·023	0·030	0·028	0·029	0·028	0·029	0·043	0·039	0·042	0·041	0·035	0·034	0·040	0·033	0·043	0·043	0·043	0·043
Ca	1·966	1·944	2·000	2·000	1·983	2·000	1·964	1·997	1·924	1·956	1·903	1·921	1·962	1·883	1·834	1·974	1·934	1·938	1·918	1·895
Na	0·034	0·056	0·000	0·000	0·017	0·000	0·036	0·003	0·076	0·044	0·097	0·079	0·038	0·117	0·166	0·026	0·066	0·062	0·082	0·105
ANa	0·465	0·381	0·181	0·164	0·247	0·218	0·212	0·190	0·234	0·194	0·162	0·183	0·213	0·142	0·034	0·153	0·202	0·147	0·199	0·164
AK	0·155	0·149	0·075	0·066	0·085	0·071	0·098	0·062	0·139	0·124	0·131	0·126	0·089	0·083	0·075	0·055	0·128	0·108	0·099	0·090
Sum A	0·620	0·530	0·279	0·264	0·332	0·289	0·309	0·252	0·373	0·318	0·292	0·309	0·302	0·225	0·109	0·208	0·330	0·256	0·299	0·254
Sum cat	15·620	15·530	15·279	15·264	15·332	15·289	15·309	15·252	15·373	15·318	15·292	15·309	15·302	15·225	15·109	15·208	15·330	15·256	15·299	15·254
Al_{total}	2·002	2·031	0·978	0·897	1·016	1·002	1·201	0·914	1·206	1·157	1·207	1·111	1·034	0·964	0·843	0·811	1·275	1·243	1·122	1·016
Fe/(Fe+Mg)	0·274	0·269	0·285	0·300	0·335	0·327	0·338	0·312	0·393	0·392	0·391	0·391	0·354	0·334	0·330	0·313	0·396	0·387	0·387	0·333

Total Fe reported as FeO. n.d., not determined; E, epidote; B, biotite; A, amphibole; Qz, quartz; D, diorite; GD, granodiorite.

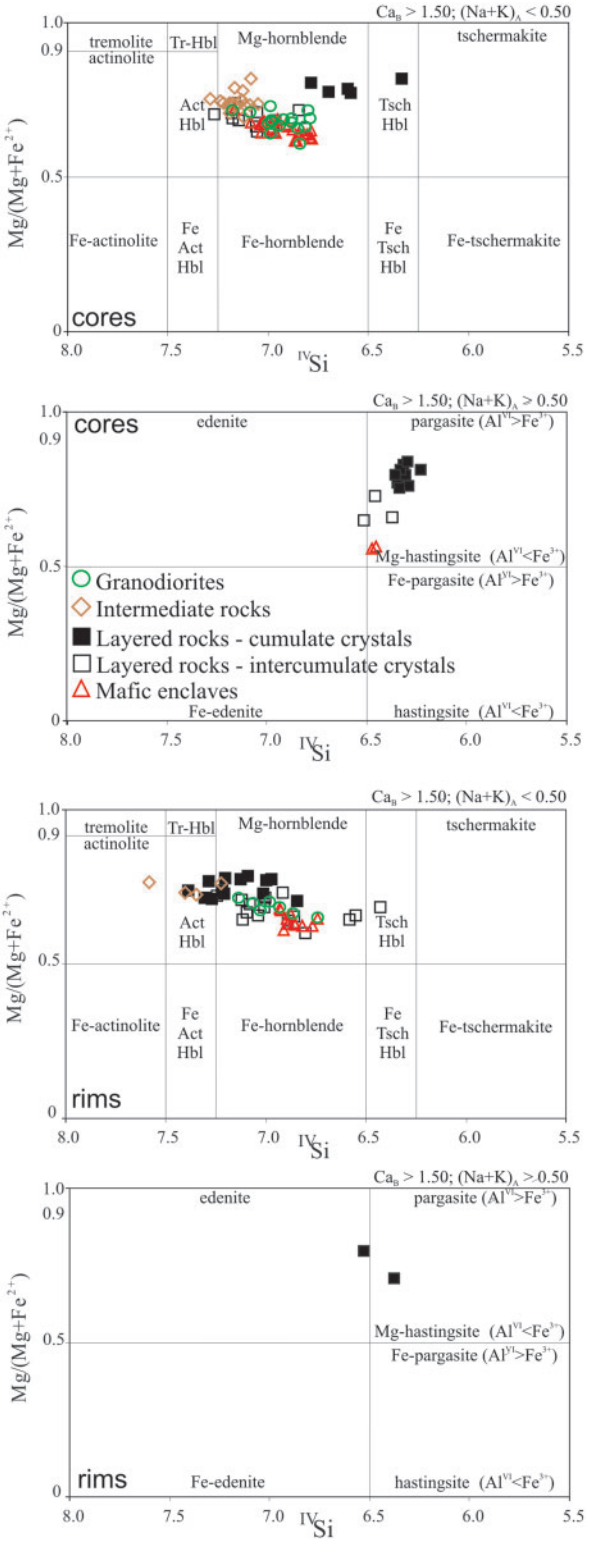

Fig. 6. Amphibole classification diagrams (Leake *et al.*, 1997) for samples of the rock units of the Rio Maria suite (Bannach area).

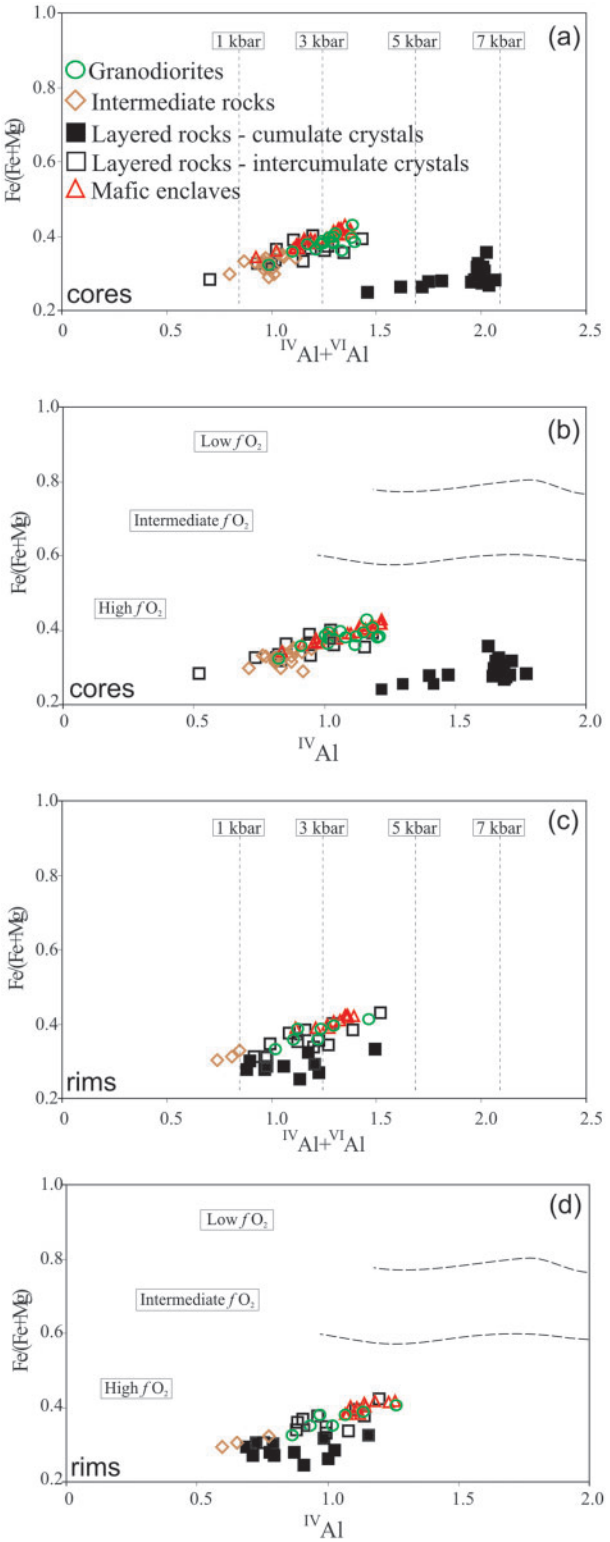

Fig. 7. (a, c) amphibole Fe/(Fe + Mg) vs Al_{tot} diagrams (Anderson & Smith, 1995) showing the possible crystallization pressures for amphibole of the Rio Maria suite; (b, d) amphibole Fe/(Fe + Mg) vs Al^{IV} diagrams (Anderson & Smith, 1995) showing the possible oxygen fugacity conditions during the crystallization of rocks of the Rio Maria suite (Bannach area).

Table 4: Representative electron microprobe analyses of biotite from the Rio Maria suite (Bannach area)

Facies	Layered rocks			Mafic enclaves			Intermediate rocks			Granodiorites		
	Intercumulus			EBAD			EBAQzD			EBAGD		
Sample:	MFR-12B	MFR-12B	MFR-12B	MFR-27C	MFR-27C	MFR-27C	ADR-4B	ADR-4B	ADR-4B	ADR-3A	ADR-3A	ADR-3A
SiO_2 (wt %)	37·213	37·753	37·820	37·308	37·322	37·648	37·330	37·384	37·878	37·400	37·534	37·759
TiO_2	1·034	1·119	1·170	1·317	1·164	1·212	0·722	0·395	0·477	1·285	1·028	1·250
Al_2O_3	15·533	16·017	15·947	15·277	15·666	15·809	16·075	16·001	16·159	15·720	15·091	14·979
FeO	14·560	15·128	13·866	18·216	18·241	18·220	15·134	14·841	14·623	16·714	16·309	15·689
MnO	0·206	0·169	0·147	0·164	0·226	0·224	0·208	0·186	0·165	0·210	0·220	0·200
MgO	14·051	13·814	13·657	12·636	12·720	12·766	14·205	14·886	14·590	12·959	13·654	13·395
CaO	0·059	0·022	0·000	0·018	0·037	0·004	0·006	0·000	0·000	0·000	0·051	0·011
Na_2O	0·009	0·053	0·041	0·069	0·108	0·117	0·029	0·108	0·122	0·177	0·075	0·109
K_2O	9·862	9·883	9·798	9·492	9·523	9·479	9·875	9·322	9·342	9·381	9·490	9·448
F	0·294	0·108	0·225	0·217	0·217	0·071	0·361	0·000	0·154	0·292	0·252	0·083
H_2O	3·857	3·948	3·891	3·895	3·896	3·966	3·826	4·000	3·926	3·859	3·878	3·960
Total	92·821	94·066	92·671	94·714	95·224	95·550	93·945	93·123	93·510	94·138	93·704	92·923
Structural formulae on the basis of 22 oxygens												
Si	5·721	5·717	5·780	5·702	5·674	5·685	5·683	5·693	5·738	5·708	5·748	5·798
Al^{IV}	2·279	2·283	2·220	2·298	2·326	2·315	2·317	2·307	2·262	2·292	2·252	2·202
Al^{VI}	0·535	0·576	0·652	0·453	0·481	0·499	0·568	0·565	0·622	0·535	0·472	0·508
Ti	0·120	0·127	0·134	0·151	0·133	0·138	0·083	0·045	0·054	0·147	0·118	0·144
Fe^{2+}	1·872	1·916	1·772	2·328	2·319	2·301	1·927	1·890	1·852	2·133	2·089	2·015
Mn	0·027	0·022	0·019	0·021	0·029	0·029	0·027	0·024	0·021	0·027	0·029	0·026
Mg	3·220	3·119	3·111	2·879	2·883	2·874	3·224	3·380	3·295	2·948	3·117	3·066
Na	0·003	0·016	0·012	0·020	0·032	0·034	0·009	0·032	0·036	0·052	0·022	0·032
K	1·934	1·909	1·910	1·851	1·847	1·826	1·918	1·811	1·805	1·826	1·854	1·851
F	0·143	0·052	0·109	0·105	0·910	0·034	0·174	0·000	0·074	0·015	0·013	0·004
Fe/(Fe + Mg)	0·368	0·381	0·363	0·447	0·446	0·445	0·374	0·359	0·360	0·420	0·401	0·397

and the host granodiorite (0·36–0·43; Fig. 7a and b). A similar pattern is observed in the amphibole rim compositions of the various studied rocks (Table 3; Fig. 7c and d).

The Al^{IV} and $Al^{IV} + Al^{VI}$ contents are very similar in the amphibole crystals of the Rio Maria suite, except for the amphibole cores of cumulate crystals in the layered rocks, which have higher Al^{IV} and total Al contents (Table 3; Fig. 7a and c). The significant difference in Al^{IV} and total Al contents between the core and rim amphibole of the cumulate crystals is remarkable (Fig. 7a and c).

Biotite

The dark mica within the rocks of the Rio Maria suite is a magnesium-biotite (Table 4; Fig. 8a, Foster, 1960; Rieder *et al.*, 1998), with Fe/(Fe + Mg) ratios (Fig. 8b) increasing from the intermediate rocks and intercumulate biotite crystals of the layered rocks (0·36–0·38), toward the granodiorite (0·40–0·42) and mafic enclaves (0·42–0·46). Fe/(Fe + Mg) ratios in coexisting hornblende and biotite are similar in the different studied rocks, except for the mafic enclaves where biotite has Fe/(Fe + Mg) ratios higher than those of the associated amphibole (Fig. 8b).

The Al contents show a narrow range, varying from 15 to 16·3 wt % (Table 4); TiO_2 contents are also low (mostly below 1·4 wt %), the lowest values being found in the intermediate rocks (0·39–0·72 wt %).

Epidote

Textural criteria described by Zen & Hammarstrom (1984) were used by Oliveira *et al.* (2009) to distinguish magmatic from secondary epidote in the rocks of the Rio Maria suite. These criteria include the presence of an allanite-rich core and chemical zoning in magmatic epidote, both

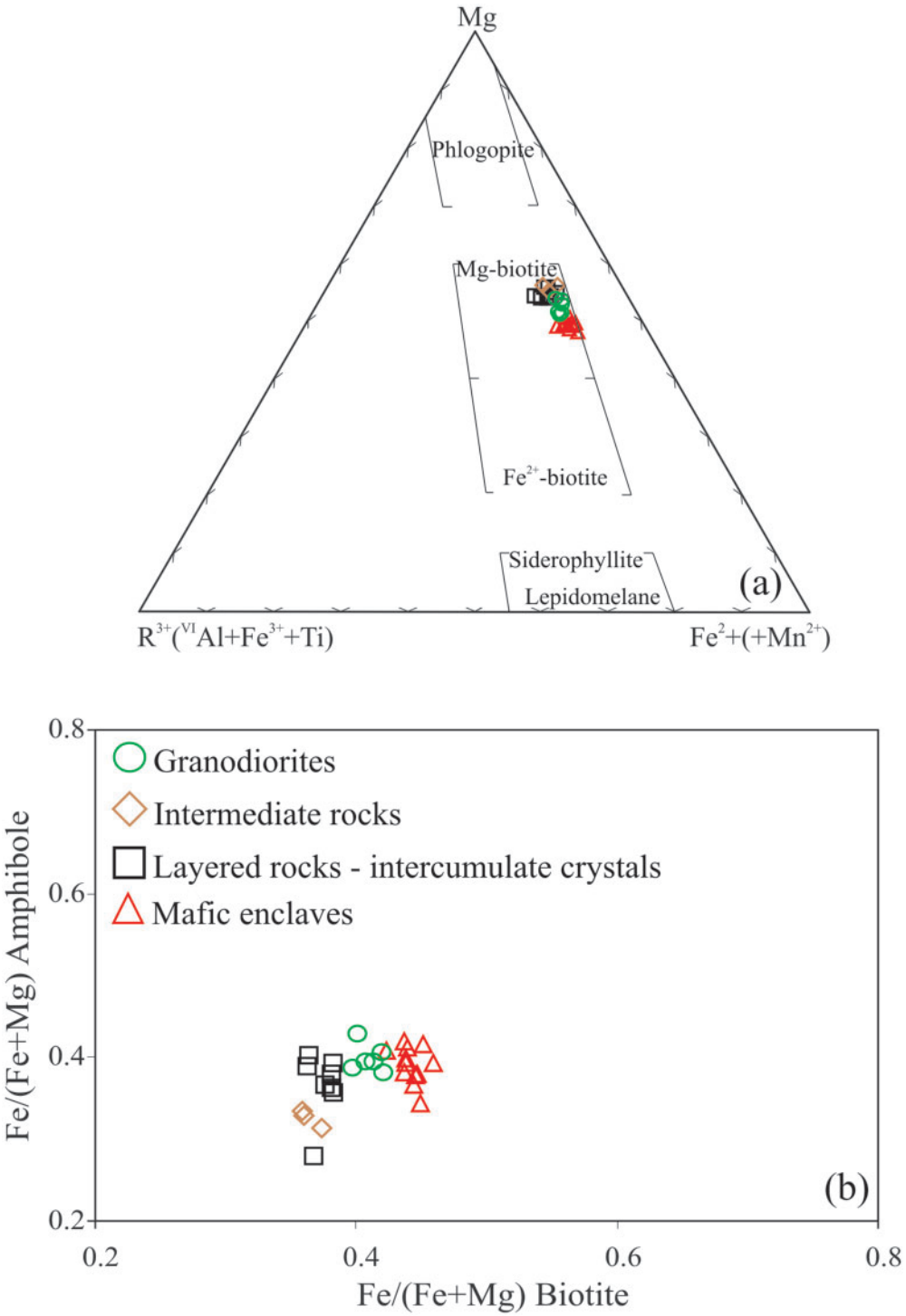

Fig. 8. (a) Mg–R^{3+}–Fe^{2+} (+Mn^{2+}) classification diagram (Foster, 1960) for micas of the rocks of the Rio Maria suite; (b) amphibole Fe/(Fe + Mg) vs biotite Fe/(Fe + Mg) plot for amphiboles and biotites of the Rio Maria suite (Bannach area).

features commonly observed in the rocks of Rio Maria suite. In the present study, additional compositional criteria (Tulloch, 1979; Evans & Vance, 1987), based on the pistacite (Ps = molar [Fe^{3+}/ (Fe^{3+} + Al)] × 100) and TiO_2 wt % content of epidote were also used to evaluate its magmatic vs subsolidus origin. More than 60 microprobe analyses of epidote crystals interpreted as magmatic on textural grounds and a few comparative analyses of

secondary epidote grains were performed. The core and rim compositions of at least eight grains per group of rocks were determined (Table 5, Fig. 9).

Euhedral epidote crystals within the Rio Maria suite have <0·2 wt % TiO_2 (Table 5), whereas epidote crystals replacing biotite have >0·6 wt % TiO_2. These results are in agreement with a magmatic and a secondary origin, respectively (Evans & Vance, 1987).

Tulloch (1979) and Vyhnal *et al.* (1991) reported pistacite contents between 25 and 29 (mol %) as typical of magmatic epidote. Tulloch (1979) also showed that epidote grains formed in the same rock by subsolidus alteration of plagioclase and biotite have $Ps_{0–24}$ and $Ps_{36–48}$, respectively (Fig. 9). In addition, analyses of synthetic epidotes by Liou (1973) indicate a pistacite content range of 25–35%. The mole per cent Ps of magmatic epidote in the Rio Maria suite lies in a narrow range $Ps_{26–33}$ (see Sial *et al.*, 1999), with a slight core-to-rim variation in Al and Fe content (Table 5). The pistacite contents of inferred magmatic epidote in the granodiorite ranges between 28 and 33. Similar values are found in the layered rocks ($Ps_{28–30}$), mafic enclaves ($Ps_{28–31}$), and intermediate rocks ($Ps_{26–31}$).

In summary, the chemical data obtained on epidote crystals from the various rocks of the Rio Maria suite and interpreted as of magmatic origin on textural grounds, show that they have pistacite and TiO_2 contents within the range expected for magmatic epidote according to previous studies (Liou, 1973; Tulloch, 1979; Vyhnal *et al.*, 1991; Sial *et al.*, 1999).

CRYSTALLIZATION PARAMETERS OF THE RIO MARIA SUITE

General considerations on the use of phase equilibria for plutonic rocks

We now first briefly review the available experimental data relevant to the petrogenesis of the Rio Maria suite, which we use here to constrain the crystallization conditions, in addition to conventional mineral geobarometers. We then combine the results of selected studies together with the petrological and mineral chemistry data presented above to provide constraints on P, T, H_2O and fO_2. A potential problem in this approach is the fact that coarse-grained igneous rocks do not represent true melt compositions, being potentially affected, *inter alia*, by mineral accumulation processes (e.g. Clemens & Wall, 1981). However, a number of experimental studies performed on plutonic rocks (e.g. Clemens & Wall, 1981; Clemens *et al.*, 1986; Scaillet *et al.*, 1995; Dall'Agnol *et al.*, 1999; Klimm *et al.*, 2003, 2008; Bogaerts *et al.*, 2006), have clearly demonstrated the usefulness of such an approach, providing, if not quantitative constraints on the intensive parameters, at least a more rigorous insight into the way the parental magmas were produced and stored. Comparison of intensive parameters obtained for volcanic and plutonic rocks, using various approaches including experimentally based ones, shows that there are no major differences between erupted and non-erupted magmas in terms of their temperature and volatile contents (Scaillet *et al.*, 1998). As an example, the experimental work on the Pinatubo dacite discussed below comes from a study of a porphyritic pumice (50% crystallized) for which cumulative processes are likely, yet inferences about its P–T–H_2O–fO_2 conditions prior to eruption have been obtained and, more importantly, the same pre-eruptive conditions have been determined using different approaches [compare Scaillet & Evans (1999) with Rutherford & Devine (1996)]. There is little doubt, therefore, that experiments can be of great help in unraveling the magmatic evolution of plutonic rocks. The convergence in estimates of magma emplacement conditions generally obtained indicates that problems related to mineral accumulation have not obscured the main magma characteristics, possibly owing to the multiply saturated nature of the system, which diminishes its variance. Lastly, we note that it is possible to retrieve basic information about magma crystallization conditions by using the conventional haplogranite system, in particular its phase relations established under various water pressures. Application of this method implies, however, two important assumptions: (1) that the magmas evolved under H_2O saturation (as the phase diagrams have been established under those conditions); (2) that the effects of components other than Si–Al–Na–K on the phase relations can be ignored. Assumption (1) has clearly no basis in the general context of Archean magmatism, and assumption (2) although permissible for Ca–Fe–Mg-poor rocks such as rhyolites or felsic granites, has no foundation either in the case of intermediate to mafic compositions such as those studied here. In particular, the elevated contents of Ca in our samples will inevitably lead to major changes in the feldspar stability fields compared with the well-known Ca-free haplogranite system. Such phase boundaries have still not been experimentally worked out, with the implication that P–T constraints derived from plotting natural (Fe–Ca–Mg-bearing) intermediate rocks in the haplogranite system are to a large extent meaningless.

Experimental studies relevant to Rio Maria Suite

A number of experimental studies have been aimed at establishing the phase equilibria and compositions of natural intermediate to silicic rocks. In Table 6 we list the starting compositions of rocks used in those studies that most closely resemble those of the Rio Maria suite. The synthetic composition of Naney (1983) has higher SiO_2, Al_2O_3, and CaO and lower Fe_2O_3 and MgO contents compared with the Rio Maria granodiorites. The composition of Schmidt & Thompson (1996) also has higher

Table 5: Representative electron microprobe analyses of epidote from the Rio Maria suite (Bannach area)

Facies:	Layered rocks						Mafic enclaves						Intermediate rocks						Granodiorites					
	Intercumulus						EBAD						EBAQzD						EBAGD					
Sample:	MFR-12B						MFR-27C						ADR-4B						ADR-3A					
	core	core	core	rim	rim	rim	core	core	core	rim	rim	rim	core	core	core	rim	rim	rim	core	core	core	rim	rim	rim
SiO_2 (wt %)	37·464	37·206	37·082	37·655	37·721	37·280	37·374	37·704	37·398	37·585	37·489	37·767	37·483	36·958	37·376	37·481	37·078	37·383	37·217	36·952	36·181	36·994	37·115	36·392
TiO_2	0·147	0·010	0·098	0·069	0·039	0·015	0·078	0·000	0·069	0·108	0·064	0·064	0·000	0·039	0·123	0·054	0·000	0·113	0·010	0·074	0·108	0·000	0·088	0·020
Al_2O_3	22·477	22·491	22·018	22·735	22·759	22·865	22·127	22·324	21·738	22·386	22·428	22·330	21·792	21·891	21·429	22·828	22·546	22·118	22·835	22·233	21·131	22·779	22·609	21·460
Fe_2O_3	13·626	14·445	14·470	13·612	14·112	14·492	14·268	14·684	14·992	13·607	14·045	15·183	14·325	14·698	15·348	12·684	14·203	13·951	14·894	15·138	16·323	14·091	15·364	16·134
MgO	0·000	0·000	0·007	0·012	0·021	0·007	0·055	0·000	0·007	0·006	0·000	0·001	0·006	0·006	0·006	0·025	0·020	0·030	0·014	0·018	0·015	0·000	0·013	0·000
CaO	23·277	22·206	22·816	23·475	22·869	23·004	22·341	23·482	22·976	23·170	22·732	22·697	22·842	22·525	22·719	22·599	21·842	22·918	22·694	23·457	22·893	23·103	23·008	22·360
MnO	0·108	0·124	0·086	0·115	0·110	0·114	0·182	0·094	0·105	0·128	0·112	0·153	0·133	0·170	0·179	0·146	0·120	0·203	0·183	0·121	0·076	0·195	0·195	0·042
Total	97·099	96·482	96·577	97·673	97·631	97·777	96·425	98·288	97·285	96·990	96·870	98·195	96·581	96·287	97·180	95·817	95·809	96·716	97·847	97·993	96·727	97·162	98·392	96·408
Number of cations on the basis of 13 oxygens																								
Si	3·135	3·132	3·128	3·133	3·138	3·103	3·136	3·128	3·137	3·148	3·142	3·133	3·158	3·128	3·142	3·161	3·138	3·143	3·099	3·085	3·076	3·099	3·083	3·092
Ti	0·009	0·001	0·006	0·004	0·003	0·001	0·005	0·000	0·004	0·007	0·004	0·004	0·000	0·003	0·008	0·003	0·000	0·007	0·001	0·005	0·007	0·000	0·006	0·001
Al	2·217	2·231	2·189	2·230	2·231	2·243	2·188	2·183	2·149	2·210	2·216	2·183	2·164	2·184	2·123	2·269	2·249	2·191	2·241	2·188	2·117	2·249	2·213	2·149
Fe^{3+}	0·858	0·915	0·919	0·852	0·883	0·908	0·901	0·917	0·946	0·858	0·886	0·948	0·908	0·936	0·971	0·805	0·905	0·883	0·933	0·951	1·044	0·888	0·960	1·032
Mg	0·000	0·000	0·001	0·002	0·003	0·001	0·007	0·000	0·001	0·001	0·000	0·000	0·001	0·001	0·001	0·003	0·003	0·004	0·002	0·002	0·002	0·000	0·002	0·000
Ca	2·087	2·003	2·062	2·093	2·038	2·052	2·009	2·087	2·065	2·079	2·041	2·018	2·062	2·043	2·046	2·042	1·981	2·064	2·025	2·098	2·085	2·074	2·047	2·035
Mn	0·008	0·009	0·006	0·008	0·008	0·008	0·013	0·007	0·008	0·009	0·008	0·011	0·010	0·012	0·013	0·010	0·009	0·015	0·013	0·009	0·006	0·014	0·014	0·003
Ps	28	29	30	28	28	29	29	30	31	28	29	30	29	30	31	26	29	29	29	30	33	28	30	32

Total Fe reported as Fe_2O_3. Ps, molar $[Fe^{3+}/(Fe^{3+} + Al)] \times 100$; E, epidote; B, biotite; A, amphibole; Qz, quartz; D, diorite; GD, granodiorite.

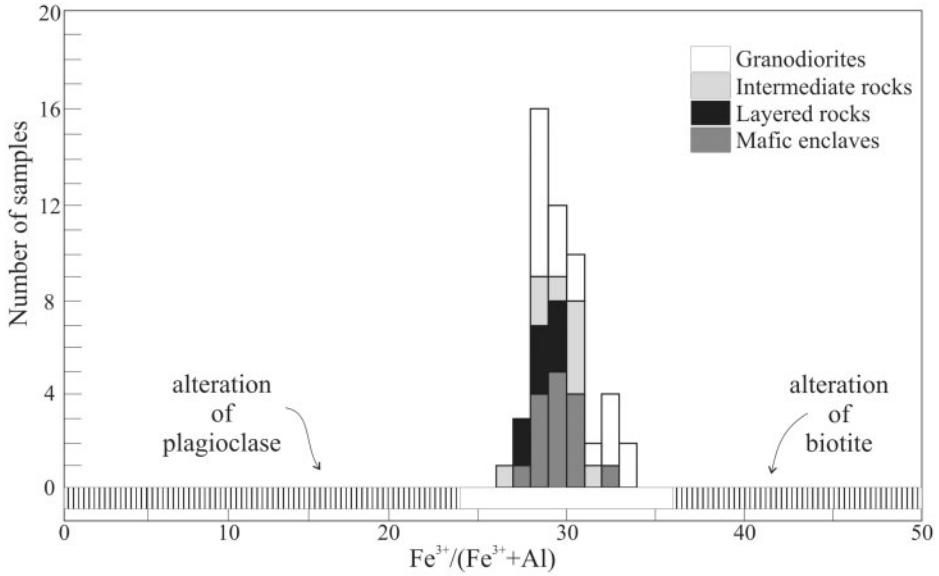

Fig. 9. Histogram of mole per cent (mol %) pistacite (Ps) in magmatic epidotes from rocks of the Rio Maria suite (Bannach area). The compositional ranges of epidote from alteration of plagioclase and biotite are from Tulloch (1979).

Table 6: Chemical composition of the starting materials (wt %) of experimental studies on similar rocks and comparison with representative samples of the Rio Maria suite (Bannach area)

	Synthetic granodiorite[1]	Alpine Adamello Granodiorite[2]	Pinatubo, 1991[3]	Lyngdal granodiorite[4]		Layered rocks[5]	Mafic enclaves[5]	Intermediate rocks[5]	Granodiorites[5]
Sample:	R5+10M	Au7	Tuff	98N50	98N06	MFR-12B	MFR-27C	ADR-4B	ADR-3A
SiO_2 (wt %)	67·51	66·66	64·60	60·20	65·20	52·60	50·51	60·51	63·9
TiO_2	0·53	0·40	0·53	1·74	1·11	0·56	0·88	0·44	0·43
Al_2O_3	17·45	15·92	16·50	13·8	14·4	10·91	16·19	14·03	14·82
FeO_t	2·20	3·28	4·37	9·26	5·80	8·91	9·01	5·56	4·27
MnO	0·10	0·11	0·10	0·16	0·10	0·15	0·13	0·09	0·06
MgO	1·19	1·58	2·39	2·15	1·39	10·51	5·65	5·37	2·39
CaO	3·52	4·43	5·23	5·35	5·50	9·3	7·61	4·73	4·02
Na_2O	3·90	2·49	4·49	3·15	3·27	2·06	4·06	4·04	4·05
K_2O	3·99	2·63	1·54	2·88	3·15	1·03	2·33	2·16	3·21
P_2O_5	–	0·12	–	0·85	0·92	0·15	0·45	0·18	0·14

Data sources: [1]Naney (1983); [2]Schmidt & Thompson (1996); [3]Pallister *et al.* (1996) used by Scaillet & Evans (1999) and Prouteau & Scaillet (2003); [4]Bogaerts *et al.* (2006); [5]Oliveira *et al.* cf. Table 2, this paper.

SiO_2, Al_2O_3, and CaO and lower Fe_2O_3 and MgO contents relative to the Rio Maria granodiorites. Of importance in the latter study is the demonstration that oxidizing conditions enhance the magmatic stability field of epidote, implying that it remains stable at higher temperatures and lower pressures relative to previous estimates (Naney, 1983; Johnston & Wyllie, 1988; Van der Laan & Wyllie, 1992). The samples selected for experimental studies of the Pinatubo dacite (Scaillet & Evans, 1999; Prouteau & Scaillet, 2003; see also Costa *et al.*, 2004) and Lyngdal granodiorite (Bogaerts *et al.*, 2006) have silica contents similar to those of the granodiorites and intermediate rocks of the Rio Maria suite (Table 6). The Pinatubo dacite resembles the Rio Maria granodiorite also in its

Table 7: Pressure estimates (in MPA) obtained by Al-in-hornblende barometry in this study

	Layered rocks				Mafic enclaves		Intermediate rocks		Granodiorites	
Facies:	Cumulate crystals		Intercumulate crystals		EBAD		EBAQzD		EBAGD	
Sample:	MFR-12B		MFR-12B		MFR-27C		ADR-4B		ADR-3A	
	core	rim	core	rim	core	rim	core	rim	core	rim
Anderson & Smith (1995)	420–745	120–300	150–405	140–450	130–340	220–350	80–215	75–90	110–290	130–320
Schmidt (1992)	400–680	115–280	145–380	135–420	140–355	230–360	90–230	85–100	170–360	180–400

E, epidote; B, biotite; A, amphibole; Qz, quartz; D, diorite; GD, granodiorite.

TiO_2, FeO_t, MgO, and Na_2O contents, differing slightly in terms of higher Al_2O_3 and CaO and, more significantly, lower K_2O contents. In contrast, the Lyngdal granodiorite differs from the Rio Maria granodiorites and intermediate rocks by its higher $FeO/(FeO+MgO)$ ratios and TiO_2 and CaO contents.

In view of the compositional differences between the Rio Maria sanukitoid rocks and those used in phase equilibrium studies, we will primarily use the phase equilibria established for the Pinatubo dacite, keeping in mind the possible distortions of the phase boundaries that may arise from minor compositional variations. The phase relations obtained in the experiments on the Pinatubo dacite, and more specifically those at pressures of 400 and 960 MPa (Prouteau & Scaillet, 2003), are indeed generally consistent with the order of crystallization deduced for the Rio Maria suite on the basis of mineralogical and petrographic studies. For epidote, a mineral phase not identified in the Pinatubo experiments, the results of other experimental studies are also considered (Naney, 1983; Schmidt & Thompson, 1996).

Pressure

Starting from the work of Hammarstrom & Zen (1986), a number of studies have shown that the total Al content of hornblende in intermediate calc-alkaline rocks increases with pressure provided that the buffering assemblage consisting of quartz, K-feldspar, plagioclase, biotite, hornblende, titanite, and Fe–Ti oxide is present (Hollister *et al.*, 1987; Johnson & Rutherford, 1989; Thomas & Ernst, 1990; Schmidt, 1992; Anderson & Smith, 1995), which is a condition fulfilled by almost the entire suite of rocks (Table 1). In this study we use the models of Schmidt (1992) and Anderson & Smith (1995), which represent the most recent experimental calibrations of this geobarometer.

The pressures calculated with these calibrations using amphibole rim compositions (Table 7) range from 100 to 300 MPa, increasing from the intermediate rocks to the mafic enclaves. Pressure estimates using core compositions gave similar results, except for the cumulate amphibole of the layered rocks which gives pressures varying from 420 to 745 MPa (Fig. 10a and b). The significance of the latter values is questionable because the cumulate amphibole crystals might not be in equilibrium with associated minerals (but see next section); yet the fact that the intercumulus amphibole of the layered rocks records pressures similar to those of the other Rio Maria sanukitoids suggests that the cores of the cumulus amphiboles formed at higher pressures relative to the intercumulus amphibole, which crystallized at the level of final emplacement at around 200 ± 100 MPa.

Another way of estimating pressure is to use the Al vs $Na+K$ and Al vs Mg-number diagrams (Prouteau & Scaillet, 2003). The Al vs $Na+K$ diagram (Fig. 10a) suggests a large range of crystallization pressures, from around 900 MPa (core composition of cumulate amphibole) down to below 200 MPa (all other amphiboles). The Al vs Mg-number diagram (Fig. 10b) suggests in turn two distinct stages of evolution: a high-pressure stage of crystallization with amphiboles clustering in the 960 MPa field with some outliers extending down to 400 MPa; a low-pressure stage of crystallization indicated by amphibole compositions (all other amphiboles) similar to those obtained in experiments at 220 MPa (Scaillet & Evans, 1999). The low-pressure amphiboles do not strictly overlap with the fields of experimental Pinatubo amphibole, but their overall lower Al_{tot} contents are indicative of low pressure of crystallization or re-equilibration at ~200 MPa, or even slightly below.

Therefore, the mineralogical evidence points to crystallization of the Rio Maria magmas involving perhaps two stages: a first high-pressure stage, possibly around 600–900 MPa, followed by a second crystallization stage at ~200 MPa, corresponding to the final emplacement of the Rio Maria magmas in the upper crust. The occurrence

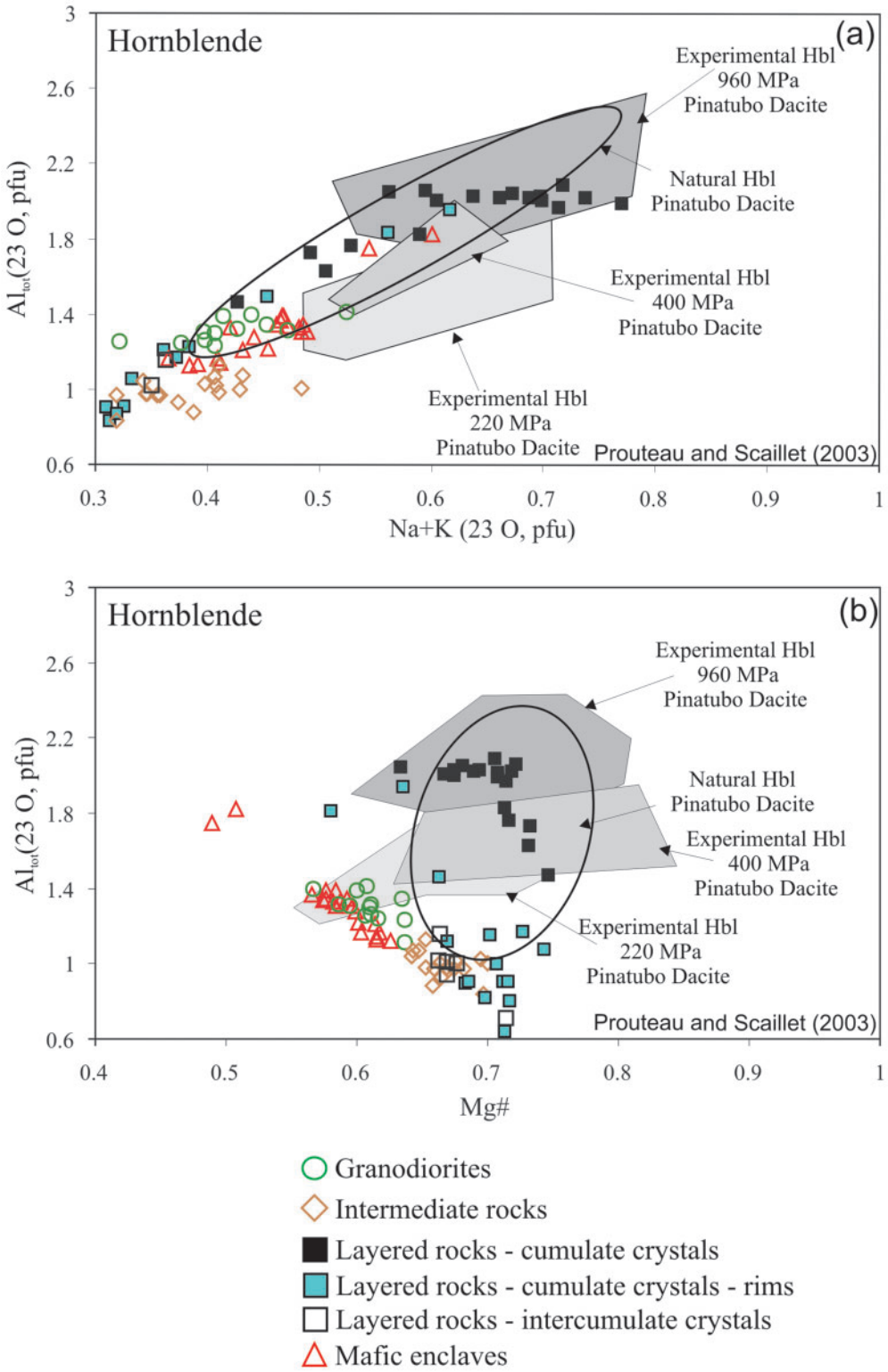

Fig. 10. Amphiboles from rocks of the Rio Maria suite (Bannach area), compared with field for natural hornblende in the 1991 Pinatubo dacite (Bernard *et al.*, 1991, 1996) and experimental amphiboles produced in the dacite system at 220 MPa (Scaillet & Evans, 1999), 400 and 960 MPa (Prouteau & Scaillet, 2003). Fields from Prouteau & Scaillet (2003).

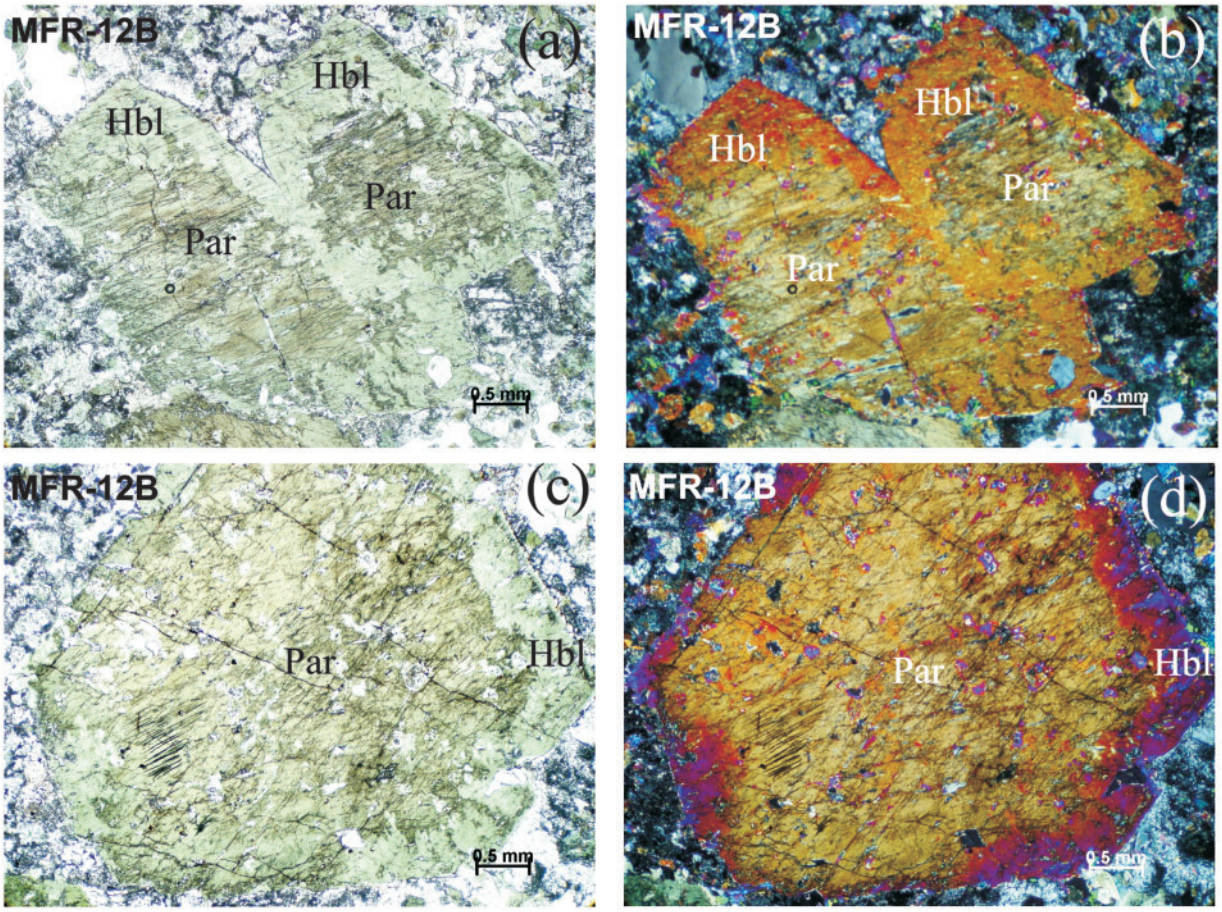

Fig. 11. Photomicrographs of centimeter-sized euhedral amphibole crystals from the layered rocks showing evidence of re-equilibration in the thin border zones. Hbl, hornblende; Par, pargasite.

of some cumulus amphibole compositions in the 400 MPa field can be interpreted as indicating either incomplete re-equilibration of the amphiboles formed at higher pressures or an intermediate level of temporary magma storage. The fact that the high-pressure stage is preserved only in the cumulate amphibole suggests the following two hypotheses: either the felsic end-member did not experience a high-pressure stage, which in turn would suggest its production (by differentiation of a mafic parental magma) at lower pressures. Alternatively, any high-pressure amphibole in the felsic rocks could have been entirely re-equilibrated at low pressure. We have no evidence for making a choice, but the fact that the compositions of the thin rims of the cumulate crystals and of the core of the intercumulate amphibole are similar to those of the other varieties of amphibole indicates that the cumulate amphibole was affected to some extent by low-pressure re-equilibration (Fig. 11). Although the compositional differences between the Pinatubo and Rio Maria rocks imply that our pressure estimates cannot be taken strictly at face value, we believe that the pressure range recorded by the compositional spread of amphibole is real, indicating crystallization across a pressure interval of at least 300 MPa.

H_2O contents and crystallization temperatures

It is now well established that the crystallization sequence of magmas in general, and the stability of amphibole in particular, are both extremely dependent on the H_2O content of the melt (e.g. Naney, 1983; Schmidt & Thompson, 1996; Scaillet & Evans, 1999; Dall'Agnol *et al.*, 1999; Klimm *et al.*, 2003; Prouteau & Scaillet, 2003; Bogaerts *et al.*, 2006; Parat *et al.*, 2008). Petrographic data for the Rio Maria suite strongly suggest the early crystallization of amphibole. Specifically, the euhedral character of the amphibole crystals, their occurrence as inclusions in quartz and alkali-feldspar, the common association with plagioclase, the absence of relicts of pyroxenes within amphibole, the presence of amphibole as the only mafic

megacryst in the layered rocks, where it is interpreted as a cumulate phase, and its elevated modal proportions (from 8 vol. % in the granodiorite to 47 vol. % in the mafic enclaves; Table 1; see also Oliveira *et al.*, 2009) are key observational features pointing toward a major role for amphibole, and hence high water contents, during magma crystallization. That some, if not all, of these features are found in all four groups of the studied rocks suggests that amphibole was a near-liquidus phase in the whole suite. In contrast, the lack of both clinopyroxene and orthopyroxene suggests that either the stability field of these phases was not crossed during crystallization, or, if pyroxenes were stable at some earlier magmatic stage, that these phases must have reacted out completely during cooling (see Naney, 1983; Dall'Agnol *et al.*, 1999). Textural relationships indicate that plagioclase was also a liquidus phase, at least in the granodiorite and intermediate rocks.

Experimental data indicate that H_2O contents of 5 wt % at 400 MPa, or 7–9 wt % at 960 MPa, are required for amphibole to be the liquidus silicate phase and to prevent the appearance of pyroxene (Naney, 1983; Prouteau & Scaillet, 2003). Therefore the widespread occurrence of amphibole in the the Rio Maria suite suggests that during the early stages of crystallization, the precursor magmas had minimum dissolved H_2O contents higher than 5 wt %, and possibly over 9 wt %, depending on pressure. Beyond its very presence, the high modal abundance of amphibole throughout the whole suite is also indicative of high water contents during magma crystallization, possibly in excess of 7 wt %. It could obviously be argued that the original modal abundances in the entire rock series have been affected to some extent by cumulative processes during magmatic differentiation. However, it is worth noting that the feldspar to amphibole ratio in many Rio Maria rocks is similar to that obtained in experimental studies performed on similar compositions: a characteristic Pl/Hbl (wt %) ratio of 2–3 is observed in the temperature range 780–850°C at 200 MPa for the Pinatubo dacite (Scaillet & Evans, 1999, see below), whose composition is close to that of the dominant Rio Maria granodiorite variety (Table 1). Similarly, the Pl/Hbl ratio in the more mafic enclaves hosted by the granodiorite is close to 0·8–1 (Table 1), which is again similar to that obtained by crystallizing a compositionnaly similar hydrous arc basalt at ~950°C and 400 MPa (Pichavant *et al.*, 2002). Therefore, if crystal sorting has occurred during magma evolution, available experimental data indicate that the cotectic mineral proportions in the precursor magmas of the Rio Maria plutonic rocks were reasonably well preserved.

Thus, it can be inferred that water-rich conditions already prevailed in the original magma(s) parental to the Rio Maria suite; that is, when the magmas had still a mafic composition. We note that the elevated melt water contents we propose are similar to those inferred for modern arc magmas of mafic to intermediate composition (e.g. Martel *et al.*, 1999; Pichavant *et al.*, 2002). Owing to the generally incompatible behavior of water in magmas, it can be anticipated that any differentiation process that has operated to produce the range of chemical variation within the Rio Maria suite probably led to an increase in the melt water content of the felsic derivatives. Additional indirect evidence of the high H_2O content of the Rio Maria sanukitoid magmas is the widespread pervasive subsolidus alteration that affected the studied rocks, responsible for the intense saussuritization of plagioclase and other associated reactions.

Constraints on magma crystallization temperatures can be made by using the Ti and Na + K contents of amphibole (Scaillet & Evans, 1999). The Ti and Na + K contents of the amphiboles from the various sanukitoid groups define a broad trend between 780 and 730°C (Fig. 12), whereas those from the layered rocks indicate a larger interval temperature, from 900 to 760°C. Although these temperature estimates are dependent on pressure in some way, they suggest that the Rio Maria sanukitoids probably began to crystallize near 950°C, extending to temperatures of ~700°C near the solidus. The lowest temperatures possibly reflect re-equilibration of near-liquidus amphibole as cooling proceeded, as well as continuous amphibole precipitation through the crystallization interval.

An additional constraint on crystallization temperatures is given by calculation of apatite saturation temperatures (Harrison & Watson, 1984). The resulting temperatures vary between 815 and 938°C and 785 and 859°C for intermediate and granodiorite rocks, respectively, overlapping with the range of crystallization temperatures derived above. For the other rock types studied, the apatite saturation temperatures are significantly higher (1085–1525°C for the mafic enclaves; 1065–1265°C for the layered rocks) possibly reflecting apatite accumulation. Zircon saturation temperatures (Watson & Harrison, 1983) are much lower than the apatite saturation temperatures. In the cases of the enclaves and the layered rocks the calculated saturation temperatures encompass the subsolidus range (590–689°C), whereas for the intermediate (676–716°C) and granodiorite (715–740°C) rocks the values approach the temperatures estimated for the solidus. The zircon saturation temperatures are, however, difficult to reconcile with the petrographic evidence for early zircon crystallization and with the temperatures inferred from experimental data and apatite thermometry.

Oxygen fugacity

Several experimental studies have shown that, at fixed T, fO_2 exerts a dominant control on the Fe/(Fe + Mg) ratio of the mafic silicates and the whole-rocks (e.g. Anderson & Smith, 1995; Dall'Agnol *et al.*, 1999; Martel *et al.*, 1999; Scaillet & Evans, 1999; Pichavant *et al.*, 2002; Prouteau &

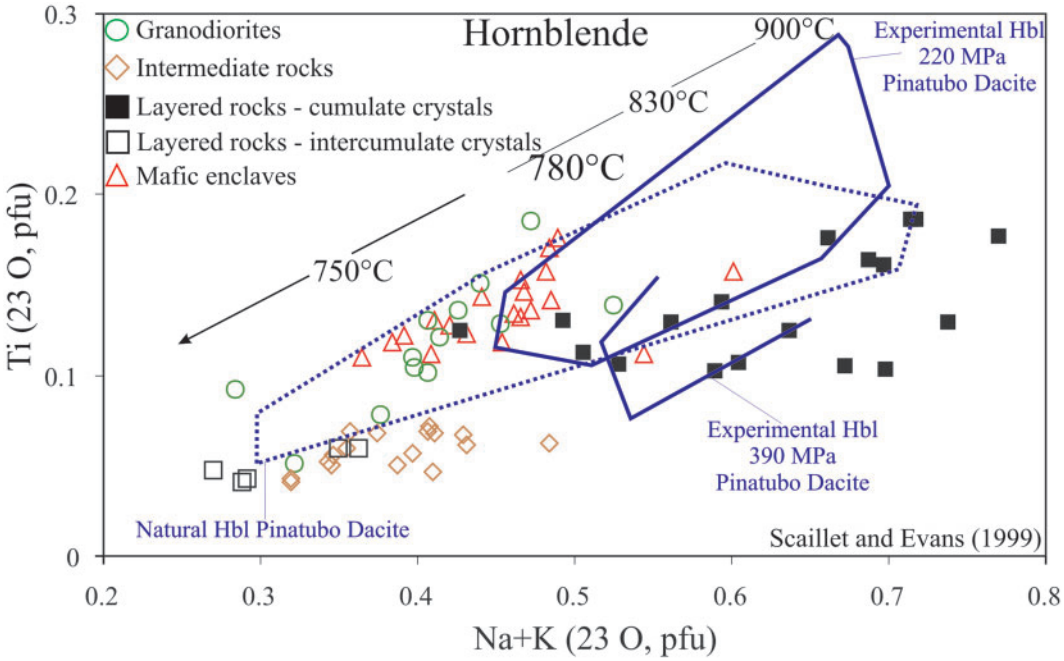

Fig. 12. Comparison of hornblende from rocks of the Rio Maria suite (Bannach area) and natural and experimental hornblende (at 220 and 390 MPa) from the Pinatubo dacite (Scaillet & Evans, 1999) in terms of Ti vs Na + K.

Scaillet, 2003; Bogaerts *et al.*, 2006). Therefore, the composition of amphibole, biotite and magmatic epidote in the studied sanukitoid rocks can be used also to evaluate the redox conditions of the Rio Maria magmas.

The Fe/(Fe + Mg) ratios in amphiboles in the layered rocks (0·25–0·43), intermediate rocks (0·25–0·35), mafic enclaves (0·34–0·43) and granodiorite (0·32–0·43) of the Rio Maria suite are relatively low. In the layered rocks, Fe/(Fe + Mg) ratios are lower in the cumulate amphibole (0·25–0·33) than in the intercumulate amphibole (0·28–0·43). The Fe/(Fe + Mg) ratio of amphibole increases from the cumulate and intermediate rocks towards the granodiorite and enclaves (Fig. 7), suggesting that the granodiorite and enclaves probably formed under slightly less oxidizing conditions relative to the cumulate and intermediate rocks. Similarly, the compositional variation of the amphibole in the layered rocks suggests that the cumulate amphibole crystallized under more oxidizing conditions than that of the intercumulus amphibole. Apart from these minor inter-group variations, amphibole compositions suggest that the Rio Maria magmas evolved under relatively oxidizing conditions, above NNO (nickel–nickel oxide) buffer (see below). This is also borne out by the relatively low whole-rock $FeO_t/(FeO_t + MgO)$ ratios of the various rocks of Rio Maria suite (Table 2), which also point to relatively oxidizing conditions (see Pichavant *et al.*, 2002). For example, the FeO_{tot}/MgO ratio of Rio Maria granodiorites is within the range 1–2 (Table 2), which is similar to that of intermediate liquids (60–64 wt % SiO_2) produced by hydrous basalt crystallization at 400 MPa at around NNO + 2 (Pichavant *et al.*, 2002).

As the Rio Maria granodiorite and Pinatubo dacite have almost identical bulk-rock Fe/Mg ratios (Table 6), the empirical relationships established between the Fe/Mg of amphibole and fO_2 for Pinatubo amphiboles by Scaillet & Evans (1999), and the data of Prouteau & Scaillet (2003), can be used to infer the redox conditions of the Rio Maria granodiorite magmas. This empirical calibration has been established at 780°C, which falls midway in the T range inferred for Rio Maria suite (Fig. 12). It can be expected that the overall positive correlation between fO_2 and Fe/Mg also holds true at other temperatures, being displaced toward higher (lower) Mg contents when temperature increases (decreases). To a first approximation, application of such a relationship to rocks with a lower Fe/Mg ratio than that of the Pinatubo dacite (i.e. all the Rio Maria suite except the granodiorites) will probably constrain the maximum possible fO_2 for amphibole crystallization. The Fe/(Fe + Mg) ratios of experimental amphibole from the Pinatubo dacite obtained at 400 MPa and 960 MPa and at an fO_2 of NNO + 2 to NNO + 4·8 (Prouteau & Scaillet, 2003) vary between 0·15 and 0·30 and are partially coincident with those of the intermediate Rio Maria rocks, but generally lower than those of the enclaves and granodiorites of the Rio Maria suite. The fact

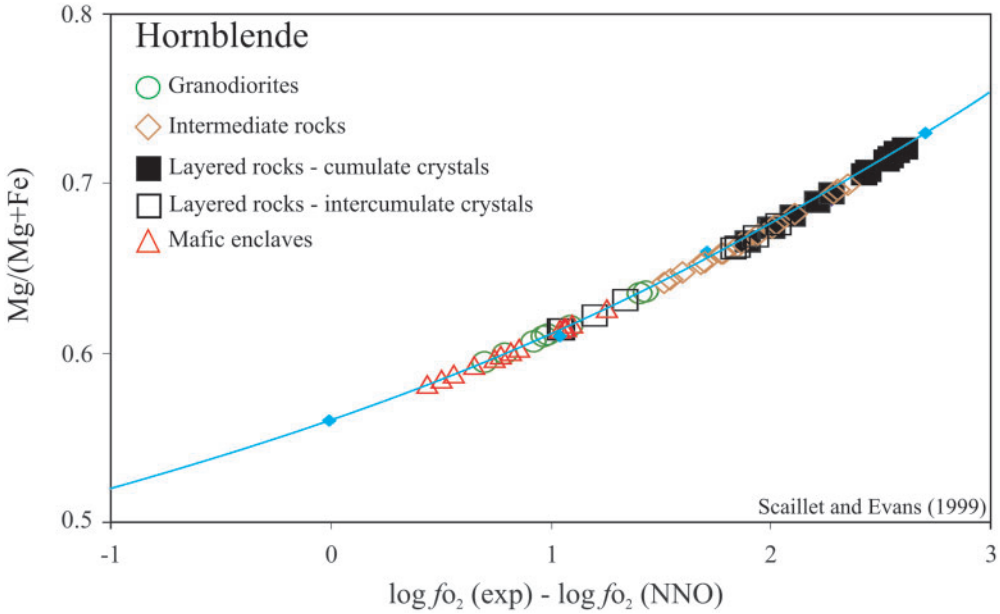

Fig. 13. Estimation of oxygen fugacity conditions of the Rio Maria magmas, based on the data of Scaillet & Evans (1999). The diagram illustrates the effect of fO_2 on the Mg-number of experimental hornblende in S-free and S-bearing dacite at 780°C and 220 MPa. The curve for hornblende in the S-free system is a second-order polynomial fit: $\Delta NNO = -20{\cdot}206 + 51{\cdot}56(\text{Mg-number}) - 27{\cdot}605(\text{Mg-number})^2$ with a correlation coefficient $r^2 = 0{\cdot}995$ (Scaillet & Evans, 1999).

that Fe/(Fe + Mg) ratios as low as 0·15 are not found in Rio Maria amphiboles suggests that the magmas evolved at fO_2 conditions less oxidized than NNO + 2, although amphiboles from both rock types partially overlap with each other. Application of the relationship of Scaillet & Evans (1999) to the Rio Maria suite thus indicates that the magmas parental to these rocks probably crystallized at relatively oxidizing conditions above the NNO buffer, yielding an overall range between NNO + 0·5 and NNO + 2·7 (Fig. 13). In detail, bearing in mind the caveats given above, the amphibole in the cumulate and intermediate rocks seems to record relatively more oxidizing conditions (NNO + 1·5 to NNO + 2·7) relative to that of the granodiorite and mafic enclaves (NNO + 0·5 to NNO + 1·4).

The Fe/(Fe + Mg) ratios of the biotite in the Rio Maria suite are slightly higher than those of amphibole (see Tables 3 and 4, and Fig. 8b) and, as for amphibole, point to relatively oxidizing conditions during the evolution of these magmas, similar to that of the Pinatubo dacite (Scaillet & Evans, 1999). The lower fO_2 recorded by biotite may arise from its greater propensity to re-equilibrate down temperature, compared with amphibole. Variations in biotite TiO_2 contents are significant and apparently related to the degree of oxidation of the parental magmas. This is suggested by the fact that the intermediate rocks have the lowest TiO_2 contents in biotite but also the lowest Fe/(Fe + Mg) ratios in biotite and amphibole [see also Dall'Agnol *et al.* (1999) for a comparable feature in the Jamon granite].

Finally, the composition of magmatic epidote can also be used to constrain the redox conditions of the Rio Maria magmas. Several studies have shown that the thermal stability of epidote increases with fO_2 (Holdaway, 1972; Liou, 1973; Schmidt & Thompson, 1996; Poli & Schmidt, 2004; Schmidt & Poli, 2004) and the Fe^{3+} content of synthetic epidote increases with fO_2 (Liou, 1973). In the Rio Maria sanukitoids, the pistacite content of magmatic epidote in the granodiorite varies between 28 and 33 mol %, whereas that in the intermediate rocks has somewhat lower values between 26 and 31 mol %. These ranges in pistacite content are achieved between the HM (hematite–magnetite) and NNO buffers (Liou, 1973), giving further support to high fO_2 conditions during the crystallization of the Rio Maria magmas (above the NNO buffer).

Lack of magnetite in oxidized magmas

As noted in the sections above, the magnetic susceptibility of the granodiorites is usually low and magnetite is rare to absent. At first sight, this could be interpreted as the typical behavior of ilmenite-series granitoids, which crystallize under low fO_2 conditions (Ishihara, 1977, 1981). However, this is in contradiction with the lack of ilmenite. A similar paradox has been observed in the

epidote-bearing granites of NE Brazil, Argentina, and Chile, which do not have magnetite as an accessory mineral, yet also show evidence of crystallization under relatively oxidizing conditions (Sial *et al.*, 1999). We thus conclude that, in the Rio Maria rocks, the magnetic susceptibility data and the nature and content of iron oxide minerals are not conclusive with respect to the oxidation conditions of the magmas. The general lack of magnetite is possibly related to its replacement by epidote during magma crystallization. When present, magnetite is found as inclusions in amphibole, indicating that it crystallized near the liquidus, along with amphibole and plagioclase. Textural evidence also suggests that epidote crystallized in equilibrium with biotite down to near-solidus conditions. These observations suggest, therefore, the operation of the following reaction (e.g. Schmidt & Thompson, 1996):

$$\begin{aligned}&\text{hornblende} + (\text{K} - \text{feldspar}_{\text{melt}})\\&\quad + \text{plagioclase} + \text{magnetite} + \text{melt}\\&\quad = \text{epidote} + \text{biotite} + (\text{quartz}_{\text{melt}}) + \text{H}_2\text{O}.\end{aligned}$$

Experimental studies have indeed shown that, for water-rich magmas ($H_2O > 4$ wt %) evolving under oxidizing conditions, early crystallizing hornblende will be replaced upon cooling by biotite- and titanite-bearing (Dall'Agnol *et al.*, 1999) or biotite- and epidote-bearing (Naney, 1983) assemblages. Hence, the abundance of magmatic epidote in the Rio Maria suite and the concomitant lack of magnetite probably originate from a peritectic reaction during cooling involving magnetite on the high-temperature side.

CONCLUSIONS AND PERSPECTIVES

Our study shows that quantitative P–T–fO_2 constraints can be obtained from the application of phase equilibria studies to fully solidified magmatic rocks, provided that the compositions of the target rocks are comparable. Insights come from the consideration not only of phase equilibria, which is a well-established approach (i.e. Maaloe & Wyllie, 1975), but also by taking into account mineral compositions, and phase proportions. The vagaries of sub-solidus modifications affecting cooling intrusions inevitably mean that errors in P–T–H_2O–fO_2 estimates for plutonic rocks are larger than for fresh volcanic rocks. However, it is worth stressing that a significant part of the observed spread reflects the fact that intensive variables governing magma evolution also vary considerably during crystallization. The case for temperature is obvious, but our work clearly shows that pressure variations can not only be documented but also estimated in a near-quantitative manner.

From the evidence presented above, we conclude that the Rio Maria magmas were water-rich, with >7 wt % water, and evolved under oxidizing conditions, above the NNO buffer, probably between NNO + 0·5 and NNO + 2·5. These conditions allowed the crystallization of amphibole as the liquidus phase, at around 950°C, inhibited clinopyroxene and orthopyroxene, and favoured crystallization of epidote at low pressure. After ascent to upper crustal levels, at around 200 MPa, plagioclase began to crystallize at around 900°C. At lower temperatures, a peritectic reaction involving amphibole + plagioclase + magnetite + ($K\text{-feldspar}_{melt}$) resulted in the precipitation of biotite and epidote. Any high-pressure amphibole should have re-equilibrated extensively at these conditions, except for the core of coarse amphibole crystals, such as those found in the cumulate rocks (Fig. 11).

The P–T–H_2O–fO_2 estimates made above for the Rio Maria suite point therefore to oxidized and wet conditions for their precursor magmas, two features characteristic of present-day arc magmas, including those with a strong slab melt signature, such as the Pinatubo magma. The immediate, and perhaps principal, implication is that sanukitoid petrogenesis at Rio Maria is indeed compatible with a subduction zone geodynamic setting during the Archean in this area. Other geodynamic interpretations are possible, however, in particular those invoking slab breakoff (Calvert *et al.*, 2004; Lobach-Zhuchenko *et al.*, 2008; Halla *et al.*, 2009). From a more general perspective, it remains to be demonstrated whether such arc attributes are specific to the Rio Maria magmas or characterize sanukitoid occurrences worldwide. The origin of the primary magmas of the Rio Maria sanukitoid rocks, as well as the level at which the granodiorite magma was produced, requires further work and will be the focus of future studies.

ACKNOWLEDGEMENTS

F. G. C. Nascimento, S. B. Dias and M. A. C. da Costa are acknowledged for their support in collection of data on magnetic susceptibility and Fe–Ti oxides. N. V. Siqueira contributed to the Fe chemical analyses. S. R. F. Vlach, E. Ruberti, and M. Mansueto are acknowledged for support in electron microprobe analyses (Institute of Geosciences of São Paulo University).

FUNDING

This research received financial support from Conselho Nacional de Desenvolvimento Científico e Tecnológico (CNPq-Brazil) (Roberto Dall'Agnol—grants 0550739/2001-7, 476075/2003-3, 307469/2003-4, 484524/2007-0; Marcelo Augusto de Oliveira—master and doctor scholarship), and the Federal University of Pará (UFPA). This paper is a contribution to the Brazilian Institute of

Amazonia Geosciences (INCT program, CNPq/MCT/FAPESPA, Process no. 573733/2008-2).

REFERENCES

Almeida, J. A. C. (2010). Geologia, Geoquímica, Geocronologia e Petrogênese das suítes TTGs e de leucogranitos arqueanos do Terreno Granito-Greenstone, sudeste do Cráton Amazônico, Doctor thesis, Centro de Geociências, UFPA, Belém, 224 p.

Althoff, F. J., Barbey, P. & Boullier, A. M. (2000). 2·8–3·0 Ga plutonism and deformation in the SE Amazonian craton: the Archean granitoids of Marajoara (Carajás Mineral province, Brazil). *Precambrian Research* **104**, 187–206.

Anderson, J. L. & Smith, D. R. (1995). The effects of temperature and fO_2 on the Al-in-hornblende barometer. *American Mineralogist* **80**, 549–559.

Bagai, Z., Armstrong, R. & Kampunzu, A. B. (2002). U–Pb single zircon geochronology of granitoids in the Vamba granite–greenstone terrane (NE Botswana): implications for the evolution of the Archaean Zimbabwe craton. *Precambrian Research* **118**, 149–168.

Barros, E. M., Sardinha, A. S., Barbosa, J. P. O., Krimski, R. & Macambira, M. J. B. (2001). Pb–Pb and U–Pb zircon ages of Archean syntectonic granites of the Carajás Metallogenic Province, northern Brazil. In: *Simposio Sudamericano de Geologia Isotopica, 3.* Pucon, Chile: Sociedade Geologica de Chile (CD ROM).

Bernard, A., Demaiffe, D., Mattielli, N. & Punongbayan, R. S. (1991). Anhydrite-bearing pumices from Mount Pinatubo: further evidence for the existence of sulfur-rich silicic magmas. *Nature* **354**, 139–140.

Bernard, A., Knittel, U., Weber, B., Weis, D., Albrecht, A., Hattori, K., Klein, J. & Oles, D. (1996). Petrology and geochemistry of the 1991 eruption products of Mount Pinatubo (Luzon, Philippines). In: Newhall, C. G. & Punongbayan, R. S. (eds) *Fire and Mud: Eruptions and Lahars of Mount Pinatubo.* Quezon City: Philippine Institute of Volcanology and Seismology; Seattle, WA: University of Washington Press, pp. 767–798.

Bogaerts, M., Scaillet, B. & Auwera, J. V. (2006). Phase equilibria of the Lyngdal granodiorite (Norway): implications for the origin of metaluminous ferroan granitoids. *Journal of Petrology* **47**, 2405–2431.

Calvert, A. J., Cruden, A. R. & Hynes, A. (2004). Seismic evidence for preservation of the Archean Uchi granite–greenstone belt by crustal scale extension. *Tectonophysics* **388**, 135–143.

Clemens, J. D. & Wall, V. J. (1981). Origin and crystallization of some peraluminous (S-type) granitic magmas. *Canadian Mineralogist* **19**, 111–131.

Clemens, J. D., Holloway, J. R. & White, A. J. R. (1986). Origin of A-type granite: experimental constraints. *American Mineralogist* **71**, 317–324.

Condie, K. C. (2005). TTGs and adakites: are they both slab melts? *Lithos* **80**, 33–44.

Costa, F., Scaillet, B. & Pichavant, M. (2004). Petrological and experimental constraints on the pre-eruptive conditions of Holocene dacite from Volcán San Pedro (36°S, Chilean Andes) and the importance of sulphur in silicic subduction-related magmas. *Journal of Petrology* **45**, 855–881.

Dall'Agnol, R. & Oliveira, D. C. (2007). Oxidized, magnetite-series, rapakivi-type granites of Carajás, Brazil: implications for classification and petrogenesis of A-type granites. *Lithos* **93**, 215–233.

Dall'Agnol, R., Scaillet, B. & Pichavant, M. (1999). An experimental study of a Lower Proterozoic A-type granite from the eastern Amazonian craton, Brazil. *Journal of Petrology* **40(11)**, 1673–1698.

Dall'Agnol, R., Teixeira, N. P., Ramö, O. T., Moura, C. A. V., Macambira, M. J. B. & Oliveira, D. C. (2005). Petrogenesis of the Paleoproterozoic rapakivi A-type granites of the Archean Carajás metallogenic province, Brazil. *Lithos* **80**, 101–129.

Dall'Agnol, R., Oliveira, M. A., Almeida, J. A. C., Althoff, F. J., Leite, A. A. S., Oliveira, D. C. & Barros, C. E. M. (2006). Archean and Paleoproterozoic granitoids of the Carajás metallogenetic province, eastern Amazonian craton. In: Dall'Agnol, R., Rosa-Costa, L. T. & Klein, E. L. (eds) *Symposium on Magmatism, Crustal Evolution, and Metallogenesis of the Amazonian Craton. Abstracts Volume and Field Trips Guide.* Belém: PRONEX-UFPA/SBG-NO, pp. 99–150.

Dias, S. B., Dall'Agnol, R. & Oliveira, M. A. (2006). Estudo dos Minerais Óxidos de Fe e Ti do Granodiorito Rio Maria e Rochas Máficas e Intermediárias Associadas, Leste de Bannach, SE do Pará. In: *XLIII Congresso Brasileiro de Geologia, 2006, Aracaju.* Brasília: Sociedade Brasileira de Geologia, 259 p.

Duarte, K. D. (1992). Geologia e geoquímica do Granito Mata Surrão (SW de Rio Maria—Pa): um exemplo de granito 'stricto sensu' Arqueano, MSc thesis, Centro de Geociências, UFPA, Belém, 217 pp.

Evans, B. W. & Vance, J. A. (1987). Epidote phenocrysts in dacitic dikes, Boulder county, Colorado. *Contributions to Mineralogy and Petrology* **96**, 178–185.

Foster, M. D. (1960). Interpretation of the composition of trioctahedral micas. *US Geological Survey, Professional Papers* **354**, 1–49.

Halla, J. (2005). Late Archean high-Mg granitoids (sanukitoids) in the southern Karelian domain, eastern Finland: Pb and Nd isotopic constraints on crust–mantle interactions. *Lithos* **79**, 161–178.

Halla, J., van Hunen, J., Heilimo, E. & Hölttä, P. (2009). Geochemical and numerical constraints on Neoarchean plate tectonics. *Precambrian Research* **179**, 155–162.

Hammarstrom, J. M. & Zen, E. (1986). Aluminum in hornblende: An empirical igneous geobarometer. *American Mineralogist* **71**, 1297–1313.

Harrison, T. M. & Watson, E. B. (1984). The behavior of apatite during crustal anatexis: Equilibrium and kinetic considerations. *Geochimica et Cosmochimica Acta* **48**, 1467–1477.

Holdaway, M. J. (1972). Thermal stability of Al–Fe-epidote as a function of fO_2, and Fe content. *Contributions to Mineralogy and Petrology* **37**, 307–340.

Hollister, L. S., Grissom, G. C., Peters, E. K., Stowell, H. H. & Sisson, V. B. (1987). Confirmation of the empirical correlation of Al in hornblende with pressure of solidification of calc-alkaline plutons. *American Mineralogist* **72**, 231–239.

Huhn, S. R. B., Santos, A. B. S., Amaral, A. F., Ledsham, E. J., Gouveia, J. L., Martins, L. B. P., Montalvão, R. M. G. & Costa, V. G. (1988). O terreno granito-greenstone da região de Rio Maria–Sul do Pará. In: *Congresso Brasileiro de Geologia, 35, Belém. Anais do congresso Brasileiro de Geologia, V. 3.* Belém: Sociedade Brasileira de Geologia, pp. 1438–1453.

Irvine, T. N. & Baragar, W. R. A. (1971). A guide to the chemical classification of the common volcanic rocks. *Canadian Journal of Earth Sciences* **8**, 523–547.

Ishihara, S. (1977). The magnetite-series and ilmenite-series granitic rocks. *Mining Geology* **27**, 293–305.

Ishihara, S. (1981). The granitoid series and mineralization. In: Skinner, B. J. (ed.) *Economic Geology*, 75th Anniversary Volume, 458–484.

Johnson, M. C. & Rutherford, M. J. (1989). Experimental calibration of the aluminum-in-hornblende geobarometer with application to Long Valley caldera (California) volcanic rocks. *Geology* **17**, 837–841.

Johnston, A. D. & Wyllie, P. J. (1988). Constraints on the origin of Archean trondhjemites based on phase relationships of Nûk gneiss with H_2O at 15 kbar. *Contributions to Mineralogy and Petrology* **100**, 35–46.

Kamber, B. S., Ewart, A., Collerson, K. D., Bruce, M. C. & McDonald, G. D. (2002). Fluid-mobile trace element constraints on the role of slab melting and implications for Archaean crustal growth models. *Contributions to Mineralogy and Petrology* **144**, 38–56.

Käpyaho, A. (2006). Whole-rock geochemistry of some tonalite and high Mg/Fe gabbro, diorite, and granodiorite plutons (sanukitoid suites) in the Kuhmo district, eastern Finland. *Bulletin of the Geological Society of Finland* **78**, 121–141.

Klimm, K., Holtz, F. & King, P. L. (2008). Fractionation vs. magma mixing in the Wangrah Suite A-type granites, Lachlan Fold Belt, Australia: Experimental constraints. *Lithos* **102**, 415–434.

Klimm, K., Holtz, F., Johannes, W. & King, P. L. (2003). Fractionation of metaluminous A-type granites: an experimental study of the Wangrah Suite, Lachlan Fold Belt, Australia. *Precambrian Research* **124**, 327–341.

Kovalenko, A. V., Clemens, J. D. & Savatenkov, V. M. (2005). Petrogenetic constraints for the genesis of Archaean sanukitoid suites: geochemistry and isotopic evidence from Karelia, Baltic Shield. *Lithos* **79**, 147–160.

Lafon, J. M., Rodrigues, E. & Duarte, K. D. (1994). Le granite Mata Surrão: un magmatisme monzogranitique contemporain des associations tonalitiques–trondhjemitiques–granodioritiques archéennes de la région de Rio Maria (Amazonie Orientale, Brésil). *Comptes Rendues de la Academie de Sciences de Paris* **318**, 642–649.

Lameyre, J. & Bowden, P. (1982). Plutonic rock type series: discrimination of various granitoid series and related rocks. *Journal of Volcanology and Geothermal Research* **14**, 169–186.

Leake, B. E., Woolley, A. R. & Arps, C. E. S. (1997). Nomenclature of amphiboles: report of the subcommittee on amphiboles of the International Mineralogical Association, commission on new minerals and mineral names. *Canadian Mineralogist* **35**, 219–246.

Leite, A. A. S. (2001). Geoquímica, petrogênese e evolução estrutural dos granitóides arqueanos da região de Xinguara, SE do Cráton Amazônico, Doctor thesis, Centro de Geociências, UFPA, Belém, 330 pp.

Leite, A. A. S., Dall'Agnol, R. & Althoff, F. J. (1999). Geoquímica e aspectos petrogenéticos do granito Xinguara, Terreno granito-greenstone de Rio Maria–Cráton Amazônico. *Revista Brasileira de Geociências* **23**, 429–436.

Leite, A. A. S., Dall'Agnol, R., Macambira, M. J. B. & Althoff, F. J. (2004). Geologia e geocronologia dos granitóides arqueanos da região de Xinguara (PA) e suas implicações na evolução do Terreno Granito-Greenstone de Rio Maria. *Revista Brasileira de Geociências* **34**, 447–458.

Lobach-Zhuchenko, S. B., Rollinson, H., Chekulaev, V. P., Savatenkov, V. M., Kovalenko., A. V., Martin, H., Guseva, N. S. & Arestova, N. A. (2008). Petrology of Late Archean, highly potassic, sanukitoid pluton from the Baltic Shield: insights into Late Archean mantle metasomatism. *Journal of Petrology* **49**, 393–420.

Maaloe, S. & Wyllie, P. J. (1975). Water content of a granite magma deduced from the sequence of crystallization determined experimentally with water-undersaturated conditions. *Contributions to Mineralogy and Petrology* **52**, 175–191.

Macambira, M. J. B. & Lafon, J. M. (1995). Geocronologia da Província Mineral de Carajás; Síntese dos dados e novos desafios. *Boletim do Museu Paraense Emílio Goeldi, série Ciências da Terra, Belém* **7**, 263–287.

Macambira, M. J. B. & Lancelot, J. (1996). Time constraints for the formation of the Archean Rio Maria crust, southeastern Amazonian Craton, Brazil. *International Geology Review* **38(12)**, 1134–1142.

Machado, N., Lindenmayer, Z. G., Krogh, T. E. & Lindenmayer, D. (1991). U–Pb geochronology of Archean magmatism and basement reactivation in the Carajás area, Amazon shield, Brazil. *Precambrian Research* **49**, 329–354.

Martel, C., Pichavant, M., Holtz, F., Scaillet, B., Bourdier, J.-L. & Traineau, H. (1999). Effects of fO_2 and H_2O on andesite phase relations between 2 and 4 kbar. *Journal of Geophysical Research* **104**, 29453–29479.

Martin, H., Smithies, R. H., Rapp, R., Moyen, J.-F. & Champion, D. (2005). An overview of adakite, tonalite–trondhjemite–granodiorite (TTG), and sanukitoid: relationships and some implications for crustal evolution. *Lithos* **79**, 1–24.

Medeiros, H. (1987). Petrologia da porção leste do maciço granodiorítico Rio Maria, Sudeste do Pará, MSc thesis, Centro de Geociências, UFPA, Belém, 166 pp.

Moyen, J. F., Martin, H., Jayananda, M. & Auvray, B. (2003). Late-Archaean granites: a typology based on the Dharwar Craton (India). *Precambrian Research* **127**, 103–123.

Naney, M. T. (1983). Phase equilibria of rock-forming ferromagnesian silicates in granitic systems. *American Journal of Science* **283**, 993–1033.

Naney, M. T. & Swanson, S. E. (1980). The effect of Fe and Mg on crystallization in granitic systems. *American Mineralogist* **65**, 639–653.

Nascimento, F. G. C. (2006). Petrologia magnética das associações magmáticas arqueanas de Canaã dos Carajás-PA, MSc thesis, Centro de Geociências, UFPA, Belém, 141 pp.

Oliveira, M. A. (2005). Geologia, Petrografia e Geoquímica do Granodiorito Sanukitóide Arqueano Rio Maria e Rochas Máficas Associadas, Leste de Bannach-PA, MSc thesis, Centro de Geociências, UFPA, Belém, 141 pp.

Oliveira, M. A., Dall'Agnol, R. & Althoff, F. J. (2006). Petrografia e Geoquímica do Granodiorito Rio Maria da região de Bannach e comparações com as demais ocorrências no terreno Granito-Greenstone de Rio Maria-Pará. *Revista Brasileira de Geociências* **36(2)**, 313–326.

Oliveira, M. A., Dall'Agnol, R., Althoff, F. J. & Leite, A. A. S. (2009). Mesoarchean sanukitoid rocks of the Rio Maria Granite–greenstone Terrane, Amazonian craton, Brazil. *Journal of South American Earth Sciences* **27**, 146–160.

Pallister, J. S., Hoblitt, R. P., Meeker, G. P., Newhall, C. G., Knight, R. J. & Siems, D. F. (1996). Magma mixing at Mount Pinatubo volcano: petrographical and chemical evidence from the 1991 deposits. In: Newhall, C. G. & Punongbayan, R. S. (eds) *Fire and Mud. Eruptions and Lahars of Mount Pinatubo, Philippines*. Quezon City: Philippine Institute of Volcanology and Seismology; Seattle: University of Washington Press, pp. 687–732.

Parat, F., Holtz, F. & Feig, S. (2008). Pre-eruptive conditions of the Huerto andesite (Fish Canyon System, San JuanVolcanic Field, Colorado): Influence of volatiles (COHS) on phase equilibria and mineral composition. *Journal of Petrology* **49**, 911–935.

Pichavant, M. & Macdonald, R. (2007). Crystallization of primitive basaltic magmas at crustal pressures and genesis of the calc-alkaline igneous suite: experimental evidence from St Vincent, Lesser Antilles arc. *Contributions to Mineralogy and Petrology* **154**, 535–558.

Pichavant, M., Martel, C., Bourdier, J.-L. & Scaillet, B. (2002). Physical conditions, structure and dynamics of a zoned magma

chamber: Mt. Peleé (Martinique, Lesser Antilles Arc). *Journal of Geophysical Research* **107**, doi:10.1029/2001JB000315.

Pichavant, M., Costa, F., Burgisser, A., Scaillet, B., Martel, C. & Poussineau, S. (2007). Equilibration scales in silicic to intermediate magmas—implications for experimental studies. *Journal of Petrology* **48**, 1955–1972.

Poli, S. & Schmidt, M. W. (2004). Experimental subsolidus studies on epidote minerals. In: Liebscher, A. & Franz, G. (eds) *Epidotes. Mineralogical Society of America and Geochemical Society, Reviews in Mineralogy and Geochemistry* **56**, 171–195.

Prouteau, G. & Scaillet, B. (2003). Experimental constraints on the origin of the 1991 Pinatubo dacite. *Journal of Petrology* **44**, 2203–2241.

Rapp, R. P., Shimizu, N., Norman, M. D. & Applegate, G. S. (1999). Reaction between slab-derived melts and peridotite in the mantle wedge: experimental constraints at 3·8 GPa. *Chemical Geology* **160**, 335–356.

Rieder, M., Cavazzini, G., D'Yakonov, Y., Frank-Kameneteskii, V. A., Gottardi, G., Guggenheim, S., Koval, P., Mueller, G., Neiva, A. M. R., Radoslovich, E. M., Robert, J., Sassi, F. P., Takeda, H., Weiss, Z. & Wones, D. R. (1998). Nomenclature of Micas. *American Mineralogist* **83**, 1366–1998.

Ringwood, A. E. (1975). *Composition and Petrology of the Earth's Mantle*. New York: McGraw–Hill, 618 p.

Rutherford, M. J. & Devine, J. (1996). Pre-eruption pressure–temperature conditions and volatiles in the 1991 Mount Pinatubo magma. In: Newhall, C. G. & Punongbayan, R. S. (eds) *Fire and Mud. Eruptions and Lahars of Mount Pinatubo, Philippines*. Quezon City: Philippine Institute of Volcanology and Seismology; Seattle: University of Washington Press, pp. 751–766.

Scaillet, B. & Evans, B. W. (1999). The June 15, 1991, eruption of Mount Pinatubo: I. Phase equilibria and pre-eruption P–T–fO_2–fH_2O conditions of the dacite magma. *Journal of Petrology* **40**, 381–411.

Scaillet, B., Pichavant, M. & Roux, J. (1995). Experimental crystallisation of leucogranite magmas. *Journal of Petrology* **36**, 663–705.

Scaillet, B., Holtz, F. & Pichavant, M. (1998). Phase equilibrium constraints on the viscosity of silicic magmas. I. Volcanic–plutonic comparison. *Journal of Geophysical Research* **103**, 27257–27266.

Schmidt, M. W. (1992). Amphibole composition in tonalite as a function of pressure: An experimental calibration of the Al-in-hornblende-barometer. *Contributions to Mineralogy and Petrology* **110**, 304–310.

Schmidt, M. W. & Poli, S. (2004). Magmatic Epidote. In: Liebscher, A. & Franz, G. (eds) *Epidotes. Mineralogical Society of America and Geochemical Society, Reviews in Mineralogy and Geochemistry* **56**, 399–430.

Schmidt, M. W. & Thompson, A. B. (1996). Epidote in calc-alkaline magmas: an experimental study of stability, phase relationships, and the role of epidote in magmatic evolution. *American Mineralogist* **81**, 424–474.

Sial, A. N., Toselli, A. J., Saavedra, J., Parada, M. A. & Ferreira, V. P. (1999). Emplacement, petrological and magnetic susceptibility characteristics of diverse magmatic epidote-bearing granitoid rocks in Brazil, Argentina and Chile. *Lithos* **46**, 367–392.

Smithies, R. H. & Champion, D. C. (2000). The Archaean high-Mg diorite suite: links to tonalite–trondhjemite–granodiorite magmatism and implications for early Archaean crustal growth. *Journal of Petrology* **41**, 1653–1671.

Souza, Z. S. (1994). Geologia e petrogênese do 'Greenstone Belt' Identidade: implicações sobre a evolução geodinâmica do terreno granito-'greenstone' de Rio Maria, SE do Pará, Doctor thesis, Centro de Geociências, UFPA, Belém, 624 pp.

Souza, Z. S. & Dall'Agnol, R. (1995). Geochemistry of metavolcanic rocks in the Archean Greenstone Belt of Identidade, SE Pará, Brazil. *Anais da Academia Brasileira de Ciências* **67**, 217–233.

Souza, Z. S., Potrel, H., Lafon, J. M., Althoff, F. J., Pimentel, M. M., Dall'Agnol, R. & Oliveira, C. G. (2001). Nd, Pb and Sr isotopes of the Identidade belt, an Archaean greenstone belt of the Rio Maria region (Carajas province, Brazil): implications for the Archaean geodynamic evolution of the Amazonian craton. *Precambrian Research* **109**, 293–315.

Stern, A. L. & Hanson, G. (1991). Archean high-Mg granodiorite: a derivate of light rare earth element-enriched monzodiorite of mantle origin. *Journal of Petrology* **32**, 201–238.

Stern, R. A., Hanson, G. N. & Shirey, S. B. (1989). Petrogenesis of mantle-derived, LILE-enriched Archean monzodiorites and trachyandesites (sanukitoids) in southwestern Superior Province. *Canadian Journal of Earth Sciences* **26**, 1688–1712.

Stevenson, R., Henry, P. & Gariépy, C. (1999). Assimilation–fractional crystallization origin of Archaean sanukitoid suites: Western Superior Province, Canada. *Precambrian Research* **96**, 83–99.

Tassinari, C. C. G. & Macambira, M. J. B. (2004). Evolução tectônica do Cráton Amazônico. In: Mantesso-Neto, V., Bartorelli, A., Carneiro, C. D. R. & de Brito Neves, B. B. (organizers) (eds) *Geologia do Continente Sul Americano: Evolução da obra de F. F. M. de Almeida*. São Paulo: BECA, pp. 471–486.

Taylor, S. R. & McLennan, S. M. (1985). *The Continental Crust: Its Composition and Evolution*. Oxford: Blackwell Scientific, 321 p.

Thomas, W. M. & Ernst, W. G. (1990). The aluminum content of hornblende in calc-alkaline granitic rocks: a mineralogic barometer calibrated experimentally to 12 kbar. In: Spencer, R. J. & Shou, I.-M. (eds) *Fluid–Mineral Interactions: A Tribute to H. P. Eugster. Geochemical Society Special Publication* **2**, 59–63.

Tulloch, A. (1979). Secondary Ca–Al silicates as low-grade alteration products of granitoid biotite. *Contributions to Mineralogy and Petrology* **69**, 105–117.

Van der Laan, S. R. & Wyllie, P. J. (1992). Constraints on Archean trondhjemite genesis from hydrous crystallization experiments on Nuk Gneiss at 10–17 kbar. *Journal of Geology* **100**, 57–68.

Vyhnal, C. R., McSween, H. Y., Jr & Speer, J. A. (1991). Hornblende chemistry in southern Appalachian granitoids: implications for aluminum hornblende thermobarometry and magmatic epidote stability. *American Mineralogist* **76**, 176–188.

Watson, E. B. & Harrison, T. M. (1983). Zircon saturation revisited: temperature and composition effects in a variety of crustal magma types. *Earth and Planetary Science Letters* **64**, 295–304.

Wilson, M. (1989). *Igneous Petrogenesis*. London: Academic Press, 466 p.

Wyllie, P. J. (1984). Sources of granitoid magmas at convergent plate boundaries. *Physics of the Earth and Planetary Interiors* **35**, 12–18.

Zen, E. & Hammarstrom, J. M. (1984). Magmatic epidote and its petrologic significance. *Geology* **12**, 515–518.